

RNF185 is required for K27-linked polyubiquitination to downregulate Ebola virus glycoprotein GP1,2 expression by reticulophagy

Jing Zhang

Harbin Veterinary Research Institute

Bin Wang

Harbin Veterinary Research Institute

Silas Johnson

Michigan State University <https://orcid.org/0000-0001-7914-1348>

Schwartz Richard

Michigan State University <https://orcid.org/0000-0003-3151-2511>

Yong-Hui Zheng (✉ zhengyo@msu.edu)

Michigan State University <https://orcid.org/0000-0002-1098-7385>

Article

Keywords: Ebola, autophagy, reticulophagy, filoviruses, calnexin, calreticulin, PDIA3

Posted Date: April 20th, 2022

DOI: <https://doi.org/10.21203/rs.3.rs-1534764/v1>

License:  This work is licensed under a Creative Commons Attribution 4.0 International License.

[Read Full License](#)

Version of Record: A version of this preprint was published at Nature Communications on October 12th, 2022. See the published version at <https://doi.org/10.1038/s41467-022-33805-9>.

Abstract

Reticulophagy reduces *Zaire* Ebolavirus (EBOV) glycoprotein GP_{1,2} expression, and thus increases viral fitness. Reticulophagy degrades endoplasmic reticulum (ER) subdomains containing misfolded proteins to restore the ER proteostasis, but whether degraded cargo proteins are polyubiquitinated is still unknown. Here, we show that the calnexin-calreticulin cycle promoted EBOV-GP_{1,2} misfolding via PDIA3/ERp57, and that misfolded GP_{1,2} was degraded via reticulophagy dependent on ATG3, ATG5, and SQSTM1/p62. EBOV-GP_{1,2} degradation also required its lysine 673 (K673), which served as a substrate for K27-linked ubiquitination. Although E3 ubiquitin ligases RNF26, RNF185, MARCH8, and TRIM25 either degraded or polyubiquitinated EBOV-GP_{1,2}, only RNF185 had both activities. Thus, RNF185 polyubiquitinates misfolded EBOV-GP_{1,2} in the ER and then SQSTM1/p62 recruits polyubiquitinated GP_{1,2} into autophagosomes for autophagic degradation. We conclude that ubiquitin is required for reticulophagy, which has played a major role in other autophagic pathways. In addition, EBOV infection should be blocked by enhanced GP_{1,2} degradation via reticulophagy.

Introduction

The endoplasmic reticulum (ER) serves as the entry site of the secretory pathway, which synthesizes ~30% of all proteins in eukaryotic cells¹. Thus, the ER must ensure the quality of native polypeptides by promoting their folding and degrading aberrant gene products. In the ER, protein disulfide isomerase family A member 3 (PDIA3/ERp57) interacts with calnexin (CANX) and calreticulin (CALR) to comprise the CANX-CALR cycle, which promotes oxidative folding of *N*-glycosylated glycoproteins by mediating disulfide bond formation². Notably, protein folding in the ER is inefficient and error-prone, resulting in accumulation of misfolded proteins that disrupts ER proteostasis³. Cells use two major degradative mechanisms to restore the ER proteostasis. Misfolded proteins can be cleared by proteasomes via ER-associated degradation (ERAD), or by lysosomes via a selected autophagy, known as reticulophagy⁴. ERAD dislocates aberrant proteins from the ER lumen to the cytosolic ubiquitin proteasome system for degradation. Reticulophagy encapsulates an ER subdomain containing misfolded proteins for lysosomal clearance via reticulophagy receptors expressed on the ER membrane. Compared to ERAD, the mechanism of reticulophagy is still poorly understood. For example, mammalian cells express over 600 ubiquitin (Ub) E3 ligases to specifically target different substrates for polyubiquitination⁵, and at least 25 of them are embedded on the ER membrane⁶. A dozen of these ER Ub ligases, such as tripartite motif containing 13 (TRIM13)⁷, Really Interesting New Gene (RING) finger protein 26 (RNF26)⁶, and RNF185⁸, have been identified to polyubiquitinate misfolded proteins during ERAD⁹. However, it is still unclear whether these E3 Ub ligases polyubiquitinate any aberrant proteins during reticulophagy.

Filoviruses are enveloped viruses with a negative-sense, single-stranded RNA genome comprising seven genes¹⁰. Two genera from this virus family, *Ebolavirus* and *Marburgvirus*, are highly pathogenic, and cause severe hemorrhagic fever in humans and nonhuman primates with up to a 90% mortality rate¹¹.

Filovirus entry is mediated by the virion-associated structural glycoprotein GP₁/GP₂ trimer, which is proteolytically processed in the Golgi apparatus from GP_{1,2} as a precursor. GP_{1,2} is expressed in the ER from the fourth gene of the viral genome, *GP*¹². Unlike GP_{1,2} from Marburg virus (MARV), high levels of GP_{1,2} expression from *Zaire* ebolavirus (EBOV) triggers cell rounding, detachment, and downregulation of many surface molecules and these cellular effects are thought to contribute to its high pathogenicity^{13, 14, 15, 16, 17, 18}. The determinants for these cellular effects are the mucin-like domain (MLD) in GP₁ and the transmembrane domain in GP₂ of EBOV^{16, 18, 19}. To balance these cellular effects against productive viral infection and spread, Ebolaviruses reduce their GP_{1,2} expression up to 70% at the mRNA levels by an RNA editing mechanism, with the vast majority of *GP* mRNAs being used to produce nonstructural soluble GP (sGP) and a small amount of small soluble GP (ssGP)^{20, 21}. The redundant sGP proteins promote immune evasion by competing for neutralizing GP_{1,2}-specific antibodies²². The sGP proteins also increase virus uptake into late endosomes by activating the mitogen-activated protein kinase (MAPK) signaling pathway²³. Thus, a low-level of GP_{1,2} expression and a high-level of sGP expression are beneficial to *Ebolavirus* by promoting viral fitness and immune evasion. We recently reported that GP_{1,2} expression is further downregulated by PDIs from the ER²⁴, which serve as another important pathway to lower the GP_{1,2} expression.

We now report that the CANX-CALR cycle promotes EBOV-GP_{1,2} misfolding via PDIA3, and that misfolded GP_{1,2} proteins are degraded via reticulophagy. GP_{1,2} degradation was dependent on autophagy-related (ATG) genes *ATG3* and *ATG5* that are required for microtubule associated protein 1 light chain 3 (MAP1LC3/LC3) lipidation. In addition, GP_{1,2} degradation was also dependent on the soluble autophagy receptor sequestosome 1 (SQSTM1/p62) that recruits polyubiquitinated cargoes. Importantly, we identified RNF185 as the key Ub ligase that polyubiquitinates EBOV-GP_{1,2} on lysine 673 (K673) in its cytoplasmic tail via K27-linked ubiquitination. We also found that RNF26 played a role in the GP_{1,2} degradation, but through a completely different mechanism. Thus, we have identified the first polyubiquitinated cargo that is targeted to reticulophagy for degradation.

Results

CANX and CALR downregulate ebolavirus GP_{1,2} expression at steady state

We identified PDIA3 as an EBOV-GP_{1,2} interacting protein in the ER by liquid chromatography tandem mass spectrometry (LC-MS/MS), resulting in discovery of EBOV-GP_{1,2} degradation via reticulophagy²⁴. In the same study, we also identified three ER chaperones, CALR, CANX, and Heat Shock Protein Family A (Hsp70) Member 5 (HSPA5), that interacted with EBOV-GP_{1,2}. To understand how these chaperones affect EBOV-GP_{1,2} expression, FLAG-tagged GP_{1,2} was expressed with HA-tagged PDIA3, HSPA5, CALR, or CANX in HEK293T cells, and their steady state expression was analyzed by western blotting (WB). GP_{1,2}

expression was strongly reduced by PDIA3, CALR, and CANX, whereas HSPA5 did not have any effect (Fig. 1A). We previously reported that PDIA3 also decreases expression of GP_{1,2} with a MLD-deletion (GP Δ MLD), but not sGP or ssGP²⁴. When CALR and CANX were expressed with these different GP forms, CANX decreased GP Δ MLD expression, whereas CALR did not (Fig. 1B, lane 3, 4, 11, 12), and neither decreased sGP and ssGP expression (Fig. 1B, lanes 5–8, 13–16). When GP interactions with CALR and CANX were tested by co-immunoprecipitation (IP), GP_{1,2}, GP Δ MLD, sGP, and ssGP all interacted with both CALR and CANX (Fig. 1C). These results demonstrate that CALR and CANX selectively downregulate GP_{1,2} expression, although they interact with all different GPs.

To validate these results, we tested the endogenous CALR and CANX activity on GP_{1,2} expression. When GP_{1,2} was expressed in HEK293T wild-type (WT), and *PDIA3*-, *CALR*-, or *CANX*-knockout (KO) cells, GP_{1,2} levels were much higher in all three KO cell lines than in the WT cell line, confirming the CALR and CANX inhibitory activity (Fig. 1D). CALR and CANX activity were further confirmed by their dose-dependent inhibition of GP_{1,2} expression in WT and their KO cell lines (Fig. 1E). Next, we tested CALR and CANX activity against GP_{1,2} proteins from the other ebolaviruses, including *Sudan* ebolavirus (SBOV), *Bundibugyo* ebolavirus (BDBV), Tai Forest ebolavirus (TAFV), and Reston ebolavirus (RESTV). Expression of these different GP_{1,2} proteins was strongly reduced by both ectopic (Fig. 1F) and endogenous (Fig. 1G) CALR and CANX. Notably, when GP_{1,2} from another filovirus, MARV, was tested, its expression was strongly increased by both ectopic and endogenous CALR and CANX (Fig. 1H). When CALR and CANX activity were further tested in several other cell lines, including A549, HeLa, Hep G2, mouse primary macrophages (M Φ), and human monocytic THP1 cell-derived macrophages (THP1-M Φ), they reduced GP_{1,2} expression to a similar level as in HEK293T cells (Fig. 1I). Collectively, these results demonstrate that CALR and CANX downregulate ebolavirus GP_{1,2} steady state expression in a cell type-independent manner.

CANX and CALR decrease EBOV entry

To understand the functional impacts of CANX and CALR activity on EBOV-GP_{1,2} expression, we used viral assays to test how EBOV entry is affected by these two ER chaperones. Initially, we used HIV-1 pseudoviruses that expressed EBOV-GP_{1,2} to measure EBOV entry, which is a standard assay for studying GP_{1,2} activity^{24, 25, 26}. Envelope glycoprotein (Env)-deficient HIV-1 luciferase reporter viruses were produced in the presence of EBOV-GP_{1,2} from HEK293T WT, and *PDIA3*-, *CALR*-, or *CANX*-overexpressing, and *PDIA3*-, *CALR*-, or *CANX*-KO cells. An equal amount of these pseudoviruses was collected to infect HEK293T cells, and viral entry was determined by measuring intracellular luciferase activity. Like *PDIA3*, ectopic CANX and CALR expression strongly decreased, whereas their KOs strongly increased EBOV entry (Fig. 2A). Next, we tested whether their inhibitory activity could be recaptured by using EBOV replication and transcription-competent virus-like particles (trVLPs), which model the entire viral replication cycle²⁷. Like *PDIA3*, both CALR and CANX consistently suppressed EBOV replication more than 10-fold in three consecutive passages (p0, p1, p2) in HEK293T cells (Fig. 2B). Furthermore, we tested how they affect GP_{1,2} levels in virions. EBOV virus-like particles (VLPs) were produced from CALR- or CANX-

overexpressing, and *CALR*- or *CANX*-KO cells after expressing EBOV-GP_{1,2} with its matrix protein VP40. Both ectopic and endogenous *CALR* and *CANX* reduced GP_{1,2} levels in these VLPs, although the endogenous protein activity was slightly weaker than the ectopic protein activity (Fig. 2C, lower panels). Finally, we tested how *CALR* and *CANX* affect expression of glycoproteins from 6 other enveloped viruses, including influenza A virus (IAV)-hemagglutinin (HA), vesicular stomatitis virus (VSV)-glycoprotein (G), HIV-1 Env, Middle East respiratory syndrome coronavirus (MERS-CoV) spike protein (S), severe acute respiratory syndrome coronavirus (SARS-CoV) S, and SARS-CoV-2 S proteins. Neither ectopic nor endogenous *CALR* and *CANX* had any noticeable effect (Fig. 2D, Fig. 2E), except that ectopic *CALR* increased VSV-G and HIV-1 Env expression (Fig. 2D, lane 5 to 8). These results demonstrate that *CALR* and *CANX* decrease EBOV entry by reducing its GP_{1,2} levels in virions, which is consistent with their downregulation of GP_{1,2} in viral producer cells.

Interrelationship between *CANX*, *CALR*, and *PDIA3* in EBOV-GP_{1,2} downregulation

CANX and *CALR* interact with *PDIA3* and promote glycoprotein folding in the ER^{28,29}. To understand their interrelationship in EBOV-GP_{1,2} downregulation, we created single *PDIA3*⁻, *CALR*⁻, or *CANX*-KO, and dual *PDIA3*/*CANX*- or *PDIA3*/*CALR*-KO cell lines from HEK293T cells (Fig. 3A). Next, EBOV-GP_{1,2} was expressed with HSPA5, *PDIA3*, *CALR*, and *CANX* in these cells, and levels of GP_{1,2} expression were compared. HSPA5 barely affected GP_{1,2} expression in any of these cells (Fig. 3B, lanes 3, 8, 13, 18, 23). In contrast, *PDIA3* (Fig. 3B, lanes 2, 7, 12, 17, 22) and *CANX* (Fig. 3B, lanes 5, 10, 15, 20, 25) strongly decreased GP_{1,2} expression in all these cells. However, *CALR* decreased GP_{1,2} expression much less effectively in the single *PDIA3*⁻ or *CANX*-KO, and dual *PDIA3*/*CANX*- or *PDIA3*/*CALR*-KO cells, although an effective decrease was detected in the single *CALR*-KO cells (Fig. 3B, lanes 4, 9, 14, 19, 24). These results demonstrate that *CALR* is dependent on *CANX* and *PDIA3*, while *CANX* is independent of *CALR* and *PDIA3* in downregulating GP_{1,2} expression. To further understand the role of PDIs in this downregulation, cells were treated with Tizoxanide (TIZ), which specifically inhibits the *PDIA3* disulfide reductase activity³⁰. Notably, GP_{1,2} downregulation by *PDIA3*, *CALR*, and *CANX* was all inhibited by TIZ in a dose-dependent manner by all three proteins (Fig. 3C). Thus, although the *CANX* activity was independent of *PDIA3*, it still requires a disulfide reductase activity to downregulate GP_{1,2}.

CANX and *CALR* target EBOV-GP_{1,2} to the autolysosomes for degradation via ERAD machinery

To understand how *CANX*/*CALR* downregulates EBOV-GP_{1,2} expression, we blocked protein degradation pathways with their respective inhibitors. First, we blocked ERAD with three inhibitors, including kifunesine (Kif), eeyarestatin I (EerI), and lactacystin (Lac). Kif inhibits the class I α -mannosidases that initiate ERAD; EerI inhibits valosin-containing protein (VCP)/p97, a member of the AAA + ATPase family that is required for retro-transportation of ERAD client proteins from the ER to the cytoplasm; and Lac

inhibits proteasomes. GP_{1,2} downregulation by CALR/CANX was blocked by Kif and Eer1 but not Lac (Fig. 4A), indicating that class I α -mannosidases and VCP/p97, but not proteasomes, are required. Second, we blocked the autolysosome activity with bafilomycin A1 (BafA1), concanamycin A (ConA), and NH₄Cl, and the proteasome activity again with MG132 and Lac. CALR and CANX activities were both blocked by autolysosome inhibitors, but not proteasome inhibitors (Fig. 4B). Third, we blocked autophagosome synthesis by 3-methyladenine (3-MA), LY 294002 (LY), and wortmannin (Wort). CALR and CANX activities were both blocked by these inhibitors (Fig. 4C).

To confirm that EBOV-GP_{1,2} is targeted by macroautophagy/autophagy, we blocked the chaperone-mediated autophagy (CMA), which requires LAMP2A (lysosomal associated membrane protein 2A) as a receptor³¹. When *LAMP2A* was silenced by small interfering RNAs (siRNAs), CALR and CANX activities were not affected (Fig. 4D). Formation of autophagosomes is dependent on a number of ATG proteins, which induce lipidation of soluble MAP1LC3/LC3-I to become LC3-II on phagophore membranes³². When LC3-II synthesis was blocked in HEK293T cells by knocking out either *ATG3* or *ATG5*, CALR and CANX activities were both blocked (Fig. 4E). We further knocked out a soluble autophagy receptor SQSTM1/p62 in HEK293T, HeLa, and A549 cells, and another autophagy receptor, histone deacetylase 6 (HDAC6) in A549 cells. CANX and CALR activities were both blocked in all three *SQSTM1*-KO cell lines (Fig. 4F), and none of them were blocked in the *HDAC6*-KO cell line (Fig. 4G). Thus, EBOV-GP_{1,2} is recruited to autophagosomes in a SQSTM1-dependent, but HDAC6-independent manner, in the presence of CANX and CALR.

To confirm that EBOV-GP_{1,2} is degraded in autolysosomes, we measured the GP_{1,2} turnover rate in the presence and absence of CANX and CALR after blocking cellular translation by cycloheximide (CHX). GP_{1,2} had a half-life of approximately 10 h, which was decreased to less than 2 h by CANX and CALR (Fig. 4H). This decrease was restored by treatment with BafA1 (Fig. 4H). We then used confocal microscopy to determine GP_{1,2} localization in autolysosomes using LAMP1 as a marker. GP_{1,2} and LAMP1 co-localization was clearly detected in the presence of CANX and CALR, which was further enhanced by treatments with BafA1 or NH₄Cl (Fig. 4I). Collectively, these results demonstrate that CANX and CALR target EBOV-GP_{1,2} to the autolysosomes for degradation via ERAD machinery.

RNF26 decreases EBOV-GP_{1,2} expression in an E3 ubiquitin ligase activity-independent manner

Our results showed that SQSTM1/p62 is required for EBOV-GP_{1,2} degradation via autophagy. To be an active autophagy receptor, SQSTM1/p62 needs to be polyubiquitinated³³. In fact, SQSTM1/p62 is polyubiquitinated by RNF26, which also tethers endosomes to the ER³⁴. In addition, RNF26 recruits the ubiquitin conjugating enzyme E2 J1 (UBE2J1) that plays an important role in ERAD^{35, 36}. Thus, we investigated the role of RNF26 in EBOV-GP_{1,2} polyubiquitination and degradation.

Initially, we investigated whether RNF26 targets EBOV-GP_{1,2}. To confirm the ER localization of RNF26, RNF26 with a C-terminal mCherry tag was expressed in HeLa cells with the ER marker CALR or the Golgi marker TGOLN2 (Trans-Golgi network integral membrane protein 2), both of which with a C-terminal GFP tag. RNF26 co-localized with CALR, but not TGOLN2, when detected by confocal microscopy (Fig. 5A). To detect the RNF26 and EBOV-GP_{1,2} interaction, EBOV-GP_{1,2} with a C-terminal GFP tag was expressed with RNF26-mCherry in HeLa cells, and their co-localization was determined by confocal microscopy. EBOV-GP_{1,2} alone was detected on the plasma membrane, but was found in the cytoplasm in the presence of RNF26 (Fig. 5B). Importantly, strong EBOV-GP_{1,2} and RNF26 co-localization was clearly detected, indicating that their interaction occurred in the ER. In addition, ectopic RNF26 strongly decreased the expression GP_{1,2} from EBOV, RSTV, SBOV, and TAFV in HEK293T cells (Fig. 5C). Thus, RNF26 targets ebolavirus GP_{1,2} and decreases its expression.

Next, we investigated how RNF26 targets EBOV-GP_{1,2}. RNF26 has 433 amino acids (aa) that comprise five transmembrane (TM) domains in the N-terminal half region and a RING-finger in the C-terminal region (Fig. 5D). We created five RNF26 deletion mutants to express its different regions that cover 76–433, 241–433, 1-385, 76–385, and 241–385 aa, and four point-mutation mutants C395S, C399S, C401S, and 3C/3S that have the critical Cys residues in the RING-finger replaced with Ser (Fig. 5D). When RNF26 WT and these mutants were expressed with EBOV-GP_{1,2} in HEK293T cells, all these RNF26 proteins were expressed at a similar level (Fig. 5E). However, unlike the others, mutants 241–433 and 241–385 did not decrease GP_{1,2} expression (Fig. 5E, lanes 4, 7). Because mutants C395S, C399S, C401S, 3C/3S, and 1-385 were still active, we conclude that the RING-finger is not required for this RNF26 activity. In addition, because mutant 76–385 was still active, whereas mutant 241–385 was not, we conclude that the 76–240 region that contains TM3, TM4, and TM5 domains is required for the RNF26 activity.

Next, we investigated how RNF26 interacts with EBOV-GP_{1,2} by co-IP. EBOV-GP_{1,2} was expressed with RNF26 WT and its mutants 76–433, 241–433, 1-385, 76–385, and 241–385, and RNF26 proteins were pulled down to detect EBOV-GP_{1,2}. RNF26 WT and its mutants 76–433, 1-385, and 76–385 pulled down EBOV-GP_{1,2}, whereas mutants 241–433 and 241–385 did not (Fig. 5F). These results confirm the RNF26 interaction with EBOV-GP_{1,2} that was suggested from the previous confocal microscopy data. In addition, they demonstrate that EBOV-GP_{1,2} interacts with RNF26 via its TM3, TM4, and TM5 domains.

Finally, we tracked the RNF26 and EBOV-GP_{1,2} interaction in live cells by bimolecular fluorescence complementation (BiFC). A basic yellow fluorescent protein Venus was divided into N-terminal (VN) and C-terminal (VC) fragments. HA-tagged VN and FLAG-tagged VC were fused to the C-terminus of RNF26 or EBOV-GP_{1,2}, respectively. Expression of RNF26-VN or GP-VC alone in cells did not produce any green fluorescence, while co-expression did produce green fluorescence (Fig. 5G). This green fluorescence colocalized with the red fluorescence produced from RNF26 after staining with fluorescent anti-HA, confirming the specificity of these BiFC signals. These BiFC signals also colocalized with CALR that has

a C-terminal blue fluorescent protein (BFP) tag (Fig. 5G). Collectively, these results confirm RNF26 downregulation of and its interaction with EBOV-GP₁,

RNF26 supports CALR, but not CANX or PDIA3 to downregulate EBOV-GP_{1,2}

To understand whether RNF26 is required for CALR, CANX, and PDIA3 activities, we knocked out *RNF26* in HEK293T cells and generated three *RNF26*-KO cell lines 1-E4, 3-B8, and 3-F10 (Fig. 6A). When EBOV-GP_{1,2} and RSTV-GP_{1,2} were expressed in WT and 1-E4 cells, levels of their GP_{1,2} expression were much higher in KO than WT cells (Fig. 6B). Thus, endogenous RNF26 also decreases GP_{1,2} expression. Next, we detected PDIA3, CALR, and CANX activities in 1-E4 cells, using WT cells as a control. PDIA3 and CANX downregulated EBOV-GP_{1,2} expression in KO cells, whereas CALR did not (Fig. 6C). We then set up a co-IP assay to test whether RNF26 interacts with PDIA3, CALR, and CANX using GFP as a control. We detected RNF26 interaction with CALR and CANX, but not PDIA3 and GFP (Fig. 6D). Lastly, we used co-IP to compare EBOV-GP_{1,2} polyubiquitination after expressing Ub in HEK293T cells in the presence of PDIA3, CALR, CANX, RNF26, and RNF26 catalytically inactive mutant 3C/3S. We detected polyubiquitinated GP_{1,2} products at above 170 kDa, which were greatly increased by PDIA3, CALR, and CANX, but not RNF26, or its mutant 3C/3S (Fig. 6E, IP, bottom panel). Collectively, our results demonstrate that RNF26 is not responsible for EBOV-GP_{1,2} polyubiquitination and selectively supports the CALR, but not CANX or PDIA3 activity.

EBOV-GP_{1,2} is polyubiquitinated with K27-linked Ub chains

To understand how EBOV-GP_{1,2} becomes polyubiquitinated, we determined the Ub chain linkage on EBOV-GP_{1,2}. Seven lysine residues within Ub can be utilized for ubiquitination (K6, K11, K27, K29, K33, K48, K63) and linkage type directs the modified proteins to different cellular fates. Initially, we generated seven Ub mutants, K6R, K11R, K27R, K29R, K33R, K48R, and K63R, where each of its seven lysine residues were individually mutated to arginine. We also generated a Ub mutant, 7K/R, in which all seven lysine residues were mutated to arginine. EBOV-GP_{1,2} was expressed with each of these Ub mutants and PDIA3, CALR, or CANX in HEK293T cells, and EBOV-GP_{1,2} polyubiquitination was analyzed again by co-IP. As we already observed, these three proteins promoted EBOV-GP_{1,2} polyubiquitination in the presence of Ub; and importantly, similar levels of polyubiquitination were detected in the presence of mutants K6R, K11R, K29R, K33R, K48R, and K63R, but not K27R and 7K/R (Fig. 7A, IP, lower panels). These results suggested that Ub K27 plays an important role in EBOV-GP_{1,2} polyubiquitination.

To confirm the important role of K27 in EBOV-GP_{1,2} polyubiquitination, we created another seven Ub mutants, K6, K11, K27, K29, K33, K48, and K63, that only express each of its seven lysine residues individually. When these mutants were used to analyze EBOV-GP_{1,2} polyubiquitination, PDIA3, CALR, and CANX promoted EBOV-GP_{1,2} polyubiquitination only in the presence of Ub and its mutant that only retains K27, but not mutants that retain K6, K11, K29, K33, K48, or K63 (Fig. 7B, IP, low panels). These results

confirm the important role of the Ub K27 residue in EBOV-GP_{1,2} polyubiquitination, suggesting that EBOV-GP_{1,2} is polyubiquitinated via K27-linked Ub chains.

RNF185 is responsible for EBOV-GP_{1,2} polyubiquitination and degradation

K27-linked ubiquitination plays an important role in the innate immune response and T cell signaling³⁷. Many E3 Ub ligases have been reported to catalyze K27-linked ubiquitination, including RNF185³⁸, membrane-associated RING-CH-type 8 (MARCH8)³⁹, and TRIM25⁴⁰. To identify the critical E3 ligase in EBOV-GP_{1,2} degradation, EBOV-GP_{1,2} and Ub were expressed with RNF185, RNF26, TRIM25, or MARCH8, and their catalytically inactive mutants 3C/3A, 3C/3S, 2E/2A, or W114A in HEK293T cells. GP_{1,2} proteins were pulled down and GP_{1,2} polyubiquitination was detected as we did previously. Among these four E3 ligases, RNF185, TRIM25, and MARCH8 strongly promoted EBOV-GP_{1,2} polyubiquitination, whereas their mutants did not, and, as we already observed, neither did RNF26 and its mutant (Fig. 8A, IP, lower panel). In addition, TRIM25 and MARCH8 did not decrease GP_{1,2} expression (Fig. 8B, lanes 7, 8). Nonetheless, MARCH8 inhibited GP_{1,2} proteolytic cleavage, as we previously reported²⁶. Notably, RNF185 decreased GP_{1,2} expression as did PDIA3, CALR, CANX, and RNF28 (Fig. 8B), whereas its mutant 3C/3A did not (Fig. 8A, Input, top panel, lanes 2, 3). Furthermore, GP_{1,2} downregulation by RNF185 was blocked by BafA1, ConA, 3-MA, Ly, and Wort, but not by Lac and MG132 (Fig. 8C, lanes 1–9). In contrast, GP_{1,2} downregulation by RNF26 was only slightly blocked by BafA1, ConA, and 3-MA, but not any other inhibitors (Fig. 8C, lanes 10–18).

RNF185 is another E3 Ub ligase on the ER membrane that plays an important role in ERAD⁴¹. Its 192 aa comprise one N-terminal RING-finger and two C-terminal TM domains (Fig. 8D). To understand how EBOV-GP_{1,2} is targeted, we created seven RNF185 deletion mutants including $\Delta 2-18$, $\Delta 19-38$, $\Delta 39-80$, $\Delta 81-132$, $\Delta 133-155$, $\Delta 171-192$, and $\Delta 133-192$, that lack the indicated regions (Fig. 8D). In addition, we created four point-mutation mutants, C39A, C42A, C79A, and 3C/3A that had the critical Cys residues in the RING-finger replaced with Ala (Fig. 8D). When RNF185 WT and these mutants were expressed with EBOV-GP_{1,2} in HEK293T cells, all these RNF26 proteins were detected by WB (Fig. 8E). Mutants $\Delta 39-80$, $\Delta 171-192$, $\Delta 133-192$, and 3C/3A did not decrease GP_{1,2} expression (Fig. 8E). These results demonstrate that the RING-finger and TM2 domain, and importantly, the E3 Ub ligase activity are all required for RNF185 downregulation of GP_{1,2} expression.

Next, we tested the RNF185 interaction with EBOV-GP_{1,2} by co-IP. EBOV-GP_{1,2} was expressed with GFP, RNF185 WT, and its mutants $\Delta 2-18$, $\Delta 19-38$, $\Delta 39-80$, $\Delta 81-132$, $\Delta 133-155$, $\Delta 171-192$, or $\Delta 133-192$ in HEK293T cells. GFP and RNF185 proteins were pulled down and their interactions with EBOV-GP_{1,2} were determined. RNF185 WT and its mutant $\Delta 133-155$ pulled down EBOV-GP_{1,2} with a similar efficiency; mutants $\Delta 2-18$, $\Delta 19-38$, and $\Delta 81-132$ pulled down EBOV-GP_{1,2} with much less efficiency; GFP and mutants $\Delta 171-192$ and $\Delta 133-192$ did not pull down any EBOV-GP_{1,2} (Fig. 8F). These results

demonstrate that EBOV-GP_{1,2} interacts with RNF185 via its TM2 domain. In addition, the 2–38 and 81–132 region that are amino terminal to the RING-finger or TM1 domain are also required for RNF185 interaction with EBOV-GP_{1,2}, likely by contributing to RNF185 structure integrity. To further validate these results, we tested whether these deletions affect RNF185 polyubiquitination activity toward EBOV-GP_{1,2}. Mutants Δ 39–80, Δ 81–132, Δ 171–192, and Δ 133–192 all showed a deficiency in promoting EBOV-GP_{1,2} polyubiquitination, as did mutant 3C/3A when compared to the WT protein (Fig. 8G), consistent with our previous results.

RNF185 polyubiquitinates EBOV-GP_{1,2} on K673 in its cytoplasmic tail

EBOV-GP_{1,2} has a very short cytoplasmic tail (CT) that only has four residues ⁶⁷³KFVF⁶⁷⁶. To determine whether K673 is targeted for polyubiquitination, we created two EBOV-GP_{1,2} mutants by replacing K673 with Ala (K673A) or deleting all these four residues (Δ CT). We found that RNF185, TRIM25, and MARCH8 could no longer polyubiquitinate mutants K673A and Δ CT (Fig. 9A, IP, lower panel). Thus, K673 is the polyubiquitination site on EBOV-GP_{1,2} for all these three E3 Ub ligases. Consistently, we also found that PDIA3, CALR, and CANX did not promote the polyubiquitination of mutants K673A and Δ CT (Fig. 9B, IP, lower panel). Finally, we determined whether these two mutants are still sensitive to those E3 ligases and ER proteins. We found that they were both resistant to MARCH8, TRIM25, RNF185, PDIA3, CALR, and CANX, although they were still as sensitive to RNF26 as was WT GP_{1,2} (Fig. 9C). To further confirm the role of RNF185 in EBOV-GP_{1,2} downregulation, we used siRNAs to knock down *RNF185* (Fig. 9D). Notably, *RNF185*-knockdown strongly increased GP_{1,2} expression (Fig. 9E). Importantly, it also disrupted GP_{1,2} downregulation by PDIA3, CALR, and CANX (Fig. 9F). Collectively, these results demonstrate that CANX-CALR cycle co-opts RNF185 to polyubiquitinate EBOV-GP_{1,2} on K673, resulting in EBOV-GP_{1,2} degradation via reticulophagy.

Discussion

So far, all known proteins targeted for reticulophagy are cellular proteins⁴². We recently reported that Ebolavirus GP_{1,2} proteins are highly vulnerable to PDIA3, even at physiological levels that more generally promote oxidative protein folding²⁴. We now show that CANX-CALR cycle indeed triggers the GP_{1,2} misfolding via PDIA3, and that misfolded GP_{1,2} proteins are targeted to reticulophagy for degradation. Thus, Ebolaviruses utilize this cellular pathway to downregulate GP_{1,2} expression and promote fitness. Importantly, Ebolavirus GP_{1,2} can be used to study the mechanism of reticulophagy that is still poorly understood.

Reticulophagy is executed through three pathways including macro-ER-phagy, micro-ER-phagy, and vesicular delivery. Macro-ER-phagy requires both the LC3 lipidation machinery and the autophagosome biogenesis machinery, and the others may only require the LC3 lipidation machinery or neither of them⁴.

The GP_{1,2} degradation by CANX/CALR was blocked by 3-Methyladenine, Wortmann, and LY294002 that block autophagosome formation by inhibiting the PI3K-III complex, and it was also blocked by knocking out *ATG-3* and *ATG-5* that are required for LC3-I lipidation. Thus, Ebolavirus GP_{1,2} proteins are degraded by the macro-ER-phagy pathway. An important question in this pathway is how misfolded proteins are segregated into an ER subdomain that is captured by autophagosomes. We reported that EBOV-GP_{1,2} proteins are targeted by ER-resident class I α -mannosidases, including MAN1B1/ERManI (mannosidase alpha class 1B member 1), EDEM1 (ER degradation enhancing α -mannosidase like 1), and EDEM2²⁴. GP_{1,2} degradation by CANX/CALR was blocked by kifunesine that specifically inhibits class I α -mannosidases and eeyarestatin I that specifically inhibits VCP/p97. Class I α -mannosidases extensively cleave α 1,2-linked mannose residues on misfolded glycoproteins in the ER, and VCP/p97 delivers demannosylated glycoproteins from the ER to the cytosolic proteasomes for degradation by ATP hydrolysis during ERAD. These results suggest that class I α -mannosidases and VCP/p97 are involved in the formation of ER subdomains that contain misfolded proteins.

Polyubiquitination plays an important role in cargo recognition during mitophagy. When mitochondria are damaged, the mitochondrial kinase PINK1 is phosphorylated to recruit the E3 Ub ligase Parkin, which in turn polyubiquitinates proteins on the mitochondrial outer membrane. Ubiquitination leads to the recruitment of soluble Sequestosome-1-like receptors (SLRs), such as SQSTM1/p62 that has a ubiquitin-associated (UBA) domain and a LC3-interacting region (LIR), and then subsequent mitophagy⁴³. We showed that GP_{1,2} degradation by CANX/CALR was blocked by knocking out *SQSTM1/p62*. In addition, it was reported that TRIM13 self-polyubiquitination is required for degradation of HSPA5 and CALR via reticulophagy⁴⁴. These results encouraged us to search for the E3 Ub ligase for EBOV-GP_{1,2} autophagic degradation. Our initial target was RNF26, which polyubiquitinates SQSTM1/p62 to liberate its UBA domain and recruit polyubiquitylated cargoes for selective autophagy^{33,34}. Although we found that RNF26 alone could decrease EBOV-GP_{1,2} expression and was required for EBOV-GP_{1,2} downregulation by CALR, it did not polyubiquitinate EBOV-GP_{1,2}. Because the RNF26 activity was only modestly blocked by autolysosome inhibitors or proteasome inhibitors, and RNF26 plays an important role in retaining lysosomes, endosomes, and vesicles in the perinuclear region of the cell³⁴, we speculate that RNF26 may directly inhibit EBOV-GP_{1,2} expression by blocking the intracellular trafficking events via its TM3, TM4, and TM5 domains.

We found that EBOV-GP_{1,2} is polyubiquitinated on K673 via K27-linked ubiquitination, which is required for its downregulation. Screening E3 Ub ligases that have such activity, we identified RNF185 as the E3 Ub ligase for EBOV-GP_{1,2} degradation. RNF185 degrades membrane proteins, such as the cystic fibrosis transmembrane conductance regulator (CFTR), ADP-ribosylation factor-like protein 6-interacting protein 5 (ARL6IP5), and human Ergosterol biosynthesis protein (Erg) 11 homolog Cytochrome P450 (CYP) 51A1 by classical ERAD that employs proteasomes for substrate degradation^{8,41,45}. In addition, RNF185 catalyzes K27-linked polyubiquitination of the cyclic GMP-AMP synthase (cGAS) and potentiates cGAS enzymatic activity that plays a key role in innate immune response³⁸. We found RNF185 not only

polyubiquitinated EBOV-GP_{1,2} on K673, but also decreased EBOV-GP_{1,2} expression via autolysosomes. All these activities required its RING-finger and E3 Ub ligase activity. We also detected RNF185 interaction with EBOV-GP_{1,2} by co-IP and mapped the interactive region to its TM1 and TM2 domains. Thus, RNF185 plays an important role in reticulophagy to degrade misfolded glycoproteins. Notably, although TRIM25 and MARCH8 polyubiquitinated EBOV-GP_{1,2} similarly, they did not downregulate EBOV-GP_{1,2}. The mechanism for this surprising result remains to be elucidated. We previously reported that MARCH8 blocks EBOV-GP_{1,2} proteolytic cleavage by furin in an E3 ligase activity-dependent manner²⁶. MARCH8 also blocked this cleavage of EBOV-GP_{1,2} mutants K673A and Δ CT (Fig. 9C, lanes 1–6). These results demonstrate that MARCH8 targets another cellular protein to inhibit furin activity.

Because CALR could not act alone, CANX played a central role in EBOV-GP_{1,2} downregulation by the CALR-CANX cycle. CANX interacts with a reticulophagy receptor RETREG1 (reticulophagy regulator 1) and the lipidated form of LC3 (LC3-II), and targets aberrant alpha1-antitrypsin Z (ATZ) and type I procollagen (PC1) to reticulophagy for degradation^{46,47}. Notably, CALR and PDIA3 are also required for clearance of PC1, but not AZT. Thus, EBOV-GP_{1,2} shares a similarity with PC1 in that CANX, CALR, and PDIA3 all play a role in the downregulation by protein degradation. Based on these observations, we propose that the CANX-RETREG1 axis plays a role in EBOV-GP_{1,2} downregulation (Fig. 10). We suggest that the CANX-CALR cycle co-opts RNF185 in the ER membrane to polyubiquitinate EBOV-GP_{1,2} on K673 via K27-linked ubiquitination in GP_{1,2} CT. Polyubiquitinated EBOV-GP_{1,2} is then recruited into autophagosomes via SQSTM1/p62 and degraded in autolysosomes. The p97-ATPase may participate in this process during invagination and pinch-off of the ER subdomains, which are captured by autophagosomes. More studies are required to further elucidate this signaling cascade. A full understanding of this novel cellular degradation pathway holds the potential for identification of new strategies for treating Ebola virus disease (EVD) by shutting down Ebolavirus GP_{1,2} expression through enhanced degradation.

Declarations

ACKNOWLEDGEMENT

We thank Eric O. Freed and Richard N. Sifers for critical reading and comments on this manuscript. We thank Ted Dawson, Feng Zhang, and Heinz Feldmann for providing reagents. BW is supported by grants from National Natural Science Foundation of China (31873013) and Natural Science Foundation of Heilongjiang Province (QC2017028).

Methods

Cell lines

Human embryonic kidney (HEK) 293 cell line transformed with SV40 large T antigen (293T), human cervical carcinoma cell line HeLa, African green monkey kidney epithelial cell line Vero E6, human lung

carcinoma cell line A549, and human hepatoblastoma cell line Hep G2 were purchased (ATCC, CRL-3216, CRM-CCL-2, CRL-1586, CRM-CCL-185). HEK293T *CALR*-KO, *CANX*-KO, and *CANX/CALR*-KO cell lines were reported²⁵. HEK293T *PDIA3*-KO, *ATG3*-KO, *ATG5*-KO, and *SQSTM1/p62*-KO cell lines, HeLa *SQSTM1/p62*-KO, and A549 *SQSTM1/p62*-KO, and *HDAC6*-KO cell lines were reported²⁴. HEK293T *RNF26*-KO, *PDIA3/CALR*-KO, and *PDIA3/CANX*-KO cell lines were generated by CRISPR/Cas9. All these cells were maintained in Dulbecco's modified Eagle medium (DMEM) (Thermo Fisher Scientific, 11965092) supplemented with 10% fetal bovine serum and 1% penicillin-streptomycin (pen-strep) (Thermo Fisher Scientific, 10378016), and cultivated at 37 °C in humidified atmosphere in a 5% CO₂ incubator.

To differentiate THP1 into macrophages (THP1-MF), human monocytic THP1 cells (ATCC, TIB-202) were grown in RPMI 1640 medium (Thermo Fisher Scientific, A4192301) supplemented with 10% FBS and 1% pen-strep in 6-well plates (1.5 × 10⁶ cells per well) and treated with 100 nM phorbol 12-myristate 13-acetate (PMA; Sigma-Aldrich, P8139) for 2 days. Primary peritoneal macrophages (MF) were isolated from mouse peritoneum and cultured in RPMI 1640 supplemented with 10% FBS and 1% pen-strep.

CRISPR-Cas9 knockout (KO) and siRNA knockdown

To create *PDIA3/CALR*-KO and *PDIA3/CANX*-KO cell lines, a DNA fragment that contained the U6 promoter, a 19-bp target sequence specific for *PDIA3*, *CALR*, or *CANX*, a small guide (sg) RNA scaffold, and a U6 termination signal sequence was synthesized and subcloned into the pGEM-T Easy vector (Promega). Two pairs of oligos were designed for *PDIA3*: 5'-TGTACAAAAAGCAGGCTT-3'/5'-GGATAAACTTTTGTGTTTCGTCCTTTCCAC-3' and 5'-AATTA AAAAGTTTATCCGTTTTAGAGCTAG-3'/5'-TAATGCCAACTTTGTACAAGAAAGCT-3'. One pair of oligos was designed for *CALR*: 5'-GGCAAGTTCTACGGTGACG-3'/5'-CGTCACCGTAGAACTTGCC-3'. One pair of oligos was designed for *CANX*: 5'-GGGTGGATTTTATCCAAAGCC-3'/5'-TCACCACAAGATTGGTCAACC-3'. The vector was transfected with a human codon-optimized Cas9 expression vector and pEGFP-C1 into HEK293T cells. Twenty-four hours later, GFP-positive cells were isolated by fluorescence-activated cell sorting (FACS) and subjected to cloning by limiting dilution. After 10-14 days, knockout clones were screened by WB.

To create *RNF26*-KO cell line, DNA oligos expressing its sgRNAs were designed and directly cloned into the pSpCas9 (BB)-2A-GFP (PX458) vector after *Bbs*I-digestion, which was obtained from Feng Zhang through Addgene (48138). Two pairs of oligos were designed to target *RNF26*: 5'-caccAGTCTTCTGCACTTGGGCCG-3'/5'-aaacCGGCCCAAGTGCAGAAGACTc-3' and 5'-caccGTTGGACCTCAACTTCTGC-3'/5'-aaacGCAGGAAGTTGAGGTCCAACc-3'. After transfection of HEK293T cells with these vectors, single GFP-positive cells were sorted out by FACS, and knockout clones were screened by WB.

LAMP2A and *RNF185* were knocked down by siRNAs using RNA oligo pairs 5'-GCACCAUGCUGGAUAUTT-3'/5'-AUAUCCAGCAUGAUGGUGCTT-3', or 5'-GUGGCUUCCAGAUGUCUUUTT-3'/5'-AAAGACAUCUGGAAGCCACTT-3'. HEK293T cells were transfected with these siRNAs, and after 24 h, their expression was determined by WB.

Expression vectors

pcDNA3.1-EBOV-GP, pcDNA3.1-EBOV-GP Δ MLD, pCMV3-EBOV-VP40, pNL-Luc- Δ Env, pMSCVneo-CANX-HA, pCMV6-CALR-Myc, and pCAGGS-CANX-HA were reported²⁵. pcDNA3.1-GFP-FLAG-HA, pRK5-Ub-His, pCAGGS-PDIA3-Myc, pCAGGS-PDIA3-HA, pcDNA3.1 vectors expressing EBOV-GP, GP Δ MLD, sGP or ssGP with a N-terminal HiBiT tag, pCAGGS-MARV-GP with a C-terminal HiBiT tag, pcDNA3.1 vectors expressing GPs from BDBV, RETV, SBOV, or TAFV with a HA-FLAG tag, and vectors expressing HIV-1 Env, IAV-H5 HA, and VSV-G were reported²⁴. pCAGGS-MARCH8-HA and its W114A mutant were reported²⁶. pEGFPC1 was from Takara.

pCMV6-CANX-Myc-FLAG was constructed from pCAGGS-CANX-HA by PCR and ASiSI/MluI digestion. pCAGGS vectors expressing MERS-CoV-S, SRAS-CoV-S, and SARS-CoV2-S with a FLAG-tag were constructed by PCR and EcoRI/XhoI digestion. pEGFPN1 vectors expressing CALR, TGLON2, and EBOV-GP were constructed by PCR and XhoI/BspEI digestion. pcDNA3.1-EBOV-GP-HA was constructed by PCR and NheI/HindIII digestion. pmBFPN1-CALR was constructed from pEGFPN1-CALR by replacing *EGFP* with *mBFP* via AgeI/NotI digestion. pRK5-HA-Ub-WT was obtained from Ted Dawson via Addgene (#17608). pCMV6-RNF26-Myc-FLAG, pCMV6-RNF185-Myc-FLAG, and pcDNA3.1-TRIM25-FLAG were ordered from CoME, ORIGENE, or JINSIRUI. pCAGGS-RNF26-mCherry was constructed from pCAGGS-ACE2-mCherry by PCR and EcoRI digestion followed by homologous recombination (Vazyme, C113-01). pcDNA3.1-RNF26-VN-HA was constructed from pcDNA3.1-ACE2-VN-HA by PCR and XhoI/BspEI digestion. pcDNA3.1-FLAG-EBOV-GP-FLAG-VC was constructed from pcDNA3.1-ACE2-FLAG-VC by PCR and XhoI/BspEI digestion. RNF26 and RNF185 deletion mutants were created by PCR and ASiSI/MluI digestion followed by homologous recombination. pcDNA3.1-FLAG-EBOV-sGP, pcDNA3.1-FLAG-EBOV-ssGP, pcDNA3.1-EBOV-GP_{1,2} K673A and Δ CT mutants, pRK5-HA-Ub mutants, and pCMV6-RNF26, pCMV6-RNF185, and pcDNA3.1-TRIM25 catalytically inactive mutants were constructed by using the QuikChange site-directed mutagenesis kit (OMEGA BIO-TEK, D6492-01). All vectors were sequenced by Sanger DNA sequencing to confirm their inserts. Detailed experimental procedures and primer sequences for construction of these vectors are available upon request. Plasmids were prepared using Maxiprep kits (TIANGEN Biotech, DP117).

Transfection

293T cells were transfected using linear 25 kDa polyethyleneimine (PEI; Polysciences, 23966-2). Briefly, to transfect cells in a 10-cm culture dish with 70% confluency, 9 mg plasmid DNAs were mixed with 27 mg PEI (stock solution at 1 mg/ml) and diluted into 500 ml Opti-MEM (Thermo Fisher Scientific, 31985062). After a 15-min incubation at room temperature, DNA-PEI complexes were added into the cell culture. After culturing cells for 4 to 6 h, cells were washed with PBS and fresh media was added for culturing another 42 h before samples were harvested. HeLa and A549 cells were transfected using Lipofectamine 3000 according to the manufacturer's protocol (Thermo Fisher Scientific, L3000).

Preparation of EBOV virus-like particles

EBOV VLPs were generated as previously²⁴. Briefly, 293T cells were transfected with EBOV-GP and EBOV-VP40 expression vectors in the presence or absence of ectopic PDIA3, CALR or CANX expression. After 48 h of transfection, the culture supernatants were collected, clarified by low-speed centrifugation, and passed through a 0.45- μ m syringe filter to remove any cell debris. To analyze the levels of EBOV GP incorporation, supernatants containing EBOV VLPs were centrifuged at 120,000 x g at 4 °C for 2 h using a Beckman SW-32Ti rotor.

Preparation of HIV-1 pseudoviruses for entry analysis

Lentiviral pseudo-virions expressing EBOV GP were generated as we did previously²⁵. Briefly, 293T cells were transfected with pNL-Luc- Δ Env and a GP-expression vector in the presence or absence of ectopic PDIA3, CALR or CANX expression. After 48 h of transfection, pseudo-virion-containing culture supernatants were collected, clarified by low-speed centrifugation, and passed through a 0.45- μ m syringe filter to remove any cell debris. After quantifying by HIV-1 p24^{Gag} ELISA, an equal number of pseudo-virions were used to infect 293T cells. After 48 h, luciferase activities were determined using Bright-Glo Luciferase Assay kit (Promega, N1130).

Production of EBOV trVLPs and infection

Experiments were performed as reported previously²⁷. EBOV trVLP vectors including p4cis-vRNA-RLuc, pCAGGS-L, pCAGGS-NP, pCAGGS-VP30, pCAGGS-VP35, pCAGGS-Tim1, and pCAGGS-T7 were provided by Heinz Feldmann (NIH). Briefly, to produce p0 trVLPs, HEK293T cells were seeded in 6-well plates at 4×10^5 per well in 2 mL medium and cultured for 24 h. EBOV trVLP system plasmids were diluted from stocks into 125 μ L Opti-MEM per well that included 125 ng pCAGGS-NP, 125 ng pCAGGS-VP35, 75 ng pCAGGS-VP30, 1,000 ng pCAGGS-L, 250 ng p4cis-vRNA-Rluc, and 250 ng pCAGGS-T7. The plasmids were combined with 7.5 μ L TransIT[®]-LT1 Transfection Reagent (Mirus Bio, 2305). After incubation at room temperature for 15 min to promote complex formation, the transfection mixes were gently added into cell culture. After 24 h of transfection, the media was exchanged for 4 mL growth media with 5% FBS, and further incubated for 72 h. All supernatants from p0 producer cells were collected followed by centrifugation at 3,000 x g for 5 min and stored at -80 °C until use. To generate p1 target cells, HEK293T cells were transfected similarly with EBOV trVLP system plasmids but had p4cis-vRNA-Rluc and pCAGGS-T7 replaced with 250 ng pCAGGS-Tim1. Transfected p1 cells were infected with p0 trVLPs, and after 72 h, p1 trVLPs were collected and stored. P2 target cells were prepared similarly and infected with p1 trVLPs. Cells from p0, p1, and p2 were lysed to quantify virus production by Renilla-Glo[®] Luciferase Assay System (Promega, E2820).

Western blotting

Cells were lysed in ice-cold RIPA lysis buffer (25 mM Tris, pH 7.4, 150 mM NaCl, 0.5% sodium deoxycholate, 0.1% SDS, 1% Nonidet P-40; Sigma-Aldrich, R0278) supplemented with protease inhibitor cocktail (Sigma-Aldrich, P8340). Approximately 0.1 mL buffer was used for a total of 2×10^6 cells. Cell

lysates was centrifuged at 12,000 x g at 4 °C for 10 min. Total protein from virion or cell extracts was boiled in SDS-polyacrylamide gel electrophoresis (SDS-PAGE) loading buffer (Solarbio Life Sciences, P1015) and resolved by SDS-PAGE. Separated proteins were transferred onto PVDF membranes and membranes were blocked with 5% non-fat milk powder in TBST (Tris-buffered saline [20 mM Tris, pH 7.4, 150 mM NaCl] containing 0.1% Tween 20; Solarbio Life Sciences, T8220) for 1 h at room temperature. Membranes were then probed by primary antibody followed by HRP-conjugated secondary antibodies. Chemiluminescence signals were then measured by incubating the membrane with SuperSignal substrate (Thermo Fisher Scientific, 34580).

Quantification of western blots

Gray analyses were performed with ImageJ software (<https://imagej.nih.gov/ij/>). Brightness and contrast were adjusted equally for all images within a panel. Levels of target proteins such as EBOV-GP or ERp57 were normalized to those of ACTB, and results were obtained from three independent experiments. Results are shown as relative values, with the value from a control (Ctrl) vector set as 1.

HiBiT blotting

Proteins were similarly separated by SDS-PAGE and transferred to a PVDF membrane. After that, proteins with HiBiT-tag were detected by Nano-Glo[®] HiBiT Blotting System (Promega, N2410). Briefly, the membrane was incubated with LgBiT/buffer solution (Promega, N2421) for 2 h at room temperature with gentle rocking and then at 4 °C overnight. The membrane was incubated with 20 µL of substrate for 5 min at room temperature and placed between transparent plastic sheets for imaging.

Immunoprecipitation

After transfection of HEK293T cells cultured in a 10-cm dish, cells were lysed in 0.9 mL RIPA lysis buffer for 30 min on ice. After removal of nuclei via low-speed centrifugation and collecting 100 µL as input, the remaining 800 µL lysate was incubated with a specific antibody followed by addition of protein G-Sepharose beads (Thermo Fisher Scientific, 22852) and rotated at 4 °C overnight. For target proteins expressing FLAG- and HA-tag, anti-FLAG M2 affinity gel (Sigma-Aldrich, A2220) or anti-HA-agarose (Sigma-Aldrich, A2095) were used for overnight rotation. After being washed 3 times with 1 mL pre-cooled RIPA lysis buffer, proteins were removed from beads after boiling in 40 µL RIPA lysis buffer plus 20 µL sample loading buffer (4[×]) and analyzed by WB.

Confocal microscopy

Approximately $1.5 \times 10^5 \sim 2.0 \times 10^5$ HeLa cells were seeded on glass bottom cell culture dish (NEST Biotechnology Co.Ltd, 801001) and transfected with various vectors using Lipofectamine 3000. After 24 h, cells were fixed with 4% paraformaldehyde, permeabilized with 0.1% Triton X-100 (Solarbio Life Sciences, T8200), and then blocked with 5% bovine serum albumin (BSA; APPLYGEN, P1622) solution. Cells were then incubated with rabbit polyclonal anti-Zaire EBOV-GP (Sino Biological, 40442-T48) at

1:1,000 dilution in PBS with 5% BSA for 2 h. After being washed 5 times with PBS, cells were stained with Alexa Fluor 488-conjugated goat anti-rabbit IgG at 1:700 dilution for 1 h. Cells were washed again with PBS 5 times and then incubated with DAPI for 3 min for nuclear staining. After further washing with PBS, cells were observed under a confocal microscope (LSM880, Zeiss, White Plains, New York). At least 100 random cells per slide were analyzed, and the most representative images from each slide were selected for presentation.

Statistical analysis

Statistical tests were performed using GraphPad Prism 8. Variance was estimated by calculating the standard error of measurements (SEMs) and represented by error bars. Significance of differences between samples was assessed using two-way ANOVA with Bonferroni post-test. All experiments were performed independently at least three times, with representative experiment being shown. * $p < 0.05$, ** $p < 0.01$, *** $p < 0.001$, **** $p < 0.0001$, ns (not significant, $p > 0.05$).

References

1. Aviram N, Schuldiner M. Targeting and translocation of proteins to the endoplasmic reticulum at a glance. *J Cell Sci* **130**, 4079–4085 (2017).
2. Kozlov G, Gehring K. Calnexin cycle - structural features of the ER chaperone system. *FEBS J* **287**, 4322–4340 (2020).
3. Hetz C. The unfolded protein response: controlling cell fate decisions under ER stress and beyond. *Nat Rev Mol Cell Biol* **13**, 89–102 (2012).
4. Molinari M. ER-phagy responses in yeast, plants, and mammalian cells and their crosstalk with UPR and ERAD. *Dev Cell* **56**, 949–966 (2021).
5. Li W, *et al.* Genome-wide and functional annotation of human E3 ubiquitin ligases identifies MULAN, a mitochondrial E3 that regulates the organelle's dynamics and signaling. *PLoS One* **3**, e1487 (2008).
6. Fenech EJ, *et al.* Interaction mapping of endoplasmic reticulum ubiquitin ligases identifies modulators of innate immune signalling. *Elife* **9**, (2020).
7. Lerner M, *et al.* The RBCC gene RFP2 (Leu5) encodes a novel transmembrane E3 ubiquitin ligase involved in ERAD. *Mol Biol Cell* **18**, 1670–1682 (2007).
8. van de Weijer ML, *et al.* Quality Control of ER Membrane Proteins by the RNF185/Membralin Ubiquitin Ligase Complex. *Mol Cell* **79**, 768–781 e767 (2020).
9. Hwang J, Qi L. Quality Control in the Endoplasmic Reticulum: Crosstalk between ERAD and UPR pathways. *Trends Biochem Sci* **43**, 593–605 (2018).
10. Hoenen T, Groseth A, Feldmann H. Therapeutic strategies to target the Ebola virus life cycle. *Nat Rev Microbiol* **17**, 593–606 (2019).
11. Feldmann H, Sprecher A, Geisbert TW. Ebola. *N Engl J Med* **382**, 1832–1842 (2020).

12. Geisbert TW. Marburg and Ebola Hemorrhagic Fevers (Filoviruses). *Mandell, Douglas, and Bennett's Principles and Practice of Infectious Diseases*, 1995–1999.e1991 (2015).
13. Francica JR, Matukonis MK, Bates P. Requirements for cell rounding and surface protein down-regulation by Ebola virus glycoprotein. *Virology* **383**, 237–247 (2009).
14. Francica JR, Varela-Rohena A, Medvec A, Plesa G, Riley JL, Bates P. Steric shielding of surface epitopes and impaired immune recognition induced by the ebola virus glycoprotein. *PLoS Pathog* **6**, e1001098 (2010).
15. Simmons G, Wool-Lewis RJ, Baribaud F, Netter RC, Bates P. Ebola virus glycoproteins induce global surface protein down-modulation and loss of cell adherence. *J Virol* **76**, 2518–2528 (2002).
16. Sullivan NJ, *et al.* Immune protection of nonhuman primates against Ebola virus with single low-dose adenovirus vectors encoding modified GPs. *PLoS Med* **3**, e177 (2006).
17. Takada A, Watanabe S, Ito H, Okazaki K, Kida H, Kawaoka Y. Downregulation of beta1 integrins by Ebola virus glycoprotein: implication for virus entry. *Virology* **278**, 20–26 (2000).
18. Yang ZY, Duckers HJ, Sullivan NJ, Sanchez A, Nabel EG, Nabel GJ. Identification of the Ebola virus glycoprotein as the main viral determinant of vascular cell cytotoxicity and injury. *Nat Med* **6**, 886–889 (2000).
19. Hacke M, *et al.* Inhibition of Ebola virus glycoprotein-mediated cytotoxicity by targeting its transmembrane domain and cholesterol. *Nat Commun* **6**, 7688 (2015).
20. Alazard-Dany N, *et al.* Ebola virus glycoprotein GP is not cytotoxic when expressed constitutively at a moderate level. *J Gen Virol* **87**, 1247–1257 (2006).
21. Volchkov VE, *et al.* Recovery of infectious Ebola virus from complementary DNA: RNA editing of the GP gene and viral cytotoxicity. *Science* **291**, 1965–1969 (2001).
22. Mohan GS, Li W, Ye L, Compans RW, Yang C. Antigenic subversion: a novel mechanism of host immune evasion by Ebola virus. *PLoS Pathog* **8**, e1003065 (2012).
23. Furuyama W, Shifflett K, Feldmann H, Marzi A. The Ebola virus soluble glycoprotein contributes to viral pathogenesis by activating the MAP kinase signaling pathway. *PLoS Pathog* **17**, e1009937 (2021).
24. Wang B, *et al.* Protein disulfide isomerases (PDIs) negatively regulate ebolavirus structural glycoprotein expression in the endoplasmic reticulum (ER) via the autophagy-lysosomal pathway. *Autophagy*, 1–18 (2022).
25. Wang B, *et al.* Mechanistic understanding of N-glycosylation in Ebola virus glycoprotein maturation and function. *J Biol Chem* **292**, 5860–5870 (2017).
26. Yu C, *et al.* MARCH8 Inhibits Ebola Virus Glycoprotein, Human Immunodeficiency Virus Type 1 Envelope Glycoprotein, and Avian Influenza Virus H5N1 Hemagglutinin Maturation. *mBio* **11**, e01882-01820 (2020).
27. Hoenen T, Watt A, Mora A, Feldmann H. Modeling the lifecycle of Ebola virus under biosafety level 2 conditions with virus-like particles containing tetracistronic minigenomes. *J Vis Exp*, 52381 (2014).

28. Frickel EM, Riek R, Jelesarov I, Helenius A, Wuthrich K, Ellgaard L. TROSY-NMR reveals interaction between ERp57 and the tip of the calreticulin P-domain. *Proc Natl Acad Sci U S A* **99**, 1954–1959 (2002).
29. Pollock S, *et al.* Specific interaction of ERp57 and calnexin determined by NMR spectroscopy and an ER two-hybrid system. *EMBO J* **23**, 1020–1029 (2004).
30. Piacentini S, *et al.* Nitazoxanide inhibits paramyxovirus replication by targeting the Fusion protein folding: role of glycoprotein-specific thiol oxidoreductase ERp57. *Sci Rep* **8**, 10425 (2018).
31. Glick D, Barth S, Macleod KF. Autophagy: cellular and molecular mechanisms. *J Pathol* **221**, 3–12 (2010).
32. Mizushima N, Yoshimori T, Ohsumi Y. The role of Atg proteins in autophagosome formation. *Annu Rev Cell Dev Biol* **27**, 107–132 (2011).
33. Peng H, *et al.* Ubiquitylation of p62/sequestosome1 activates its autophagy receptor function and controls selective autophagy upon ubiquitin stress. *Cell Res* **27**, 657–674 (2017).
34. Jongsma ML, *et al.* An ER-Associated Pathway Defines Endosomal Architecture for Controlled Cargo Transport. *Cell* **166**, 152–166 (2016).
35. Cremer T, Jongsma MLM, Trulsson F, Vertegaal ACO, Neefjes J, Berlin I. The ER-embedded UBE2J1/RNF26 ubiquitylation complex exerts spatiotemporal control over the endolysosomal pathway. *Cell Rep* **34**, 108659 (2021).
36. Hagiwara M, Ling J, Koenig PA, Ploegh HL. Posttranscriptional Regulation of Glycoprotein Quality Control in the Endoplasmic Reticulum Is Controlled by the E2 Ub-Conjugating Enzyme UBC6e. *Mol Cell* **63**, 753–767 (2016).
37. Zhou Q, Zhang J. K27-linked noncanonical ubiquitination in immune regulation. *J Leukoc Biol* **111**, 223–235 (2022).
38. Wang Q, *et al.* The E3 ubiquitin ligase RNF185 facilitates the cGAS-mediated innate immune response. *PLoS Pathog* **13**, e1006264 (2017).
39. Jin S, *et al.* Tetherin Suppresses Type I Interferon Signaling by Targeting MAVS for NDP52-Mediated Selective Autophagic Degradation in Human Cells. *Mol Cell* **68**, 308–322 e304 (2017).
40. Wang S, *et al.* TRIM25 inhibits infectious bursal disease virus replication by targeting VP3 for ubiquitination and degradation. *PLoS Pathog* **17**, e1009900 (2021).
41. El Khouri E, Le Pavec G, Toledano MB, Delaunay-Moisan A. RNF185 is a novel E3 ligase of endoplasmic reticulum-associated degradation (ERAD) that targets cystic fibrosis transmembrane conductance regulator (CFTR). *J Biol Chem* **288**, 31177–31191 (2013).
42. Chino H, Mizushima N. ER-Phagy: Quality Control and Turnover of Endoplasmic Reticulum. *Trends Cell Biol* **30**, 384–398 (2020).
43. Lamark T, Johansen T. Mechanisms of Selective Autophagy. *Annu Rev Cell Dev Biol* **37**, 143–169 (2021).
44. Ji CH, *et al.* The N-Degron Pathway Mediates ER-phagy. *Mol Cell* **75**, 1058–1072 e1059 (2019).

45. Qiu D, *et al.* RNF185 modulates JWA ubiquitination and promotes gastric cancer metastasis. *Biochim Biophys Acta Mol Basis Dis* **1864**, 1552–1561 (2018).
46. Forrester A, *et al.* A selective ER-phagy exerts procollagen quality control via a Calnexin-FAM134B complex. *EMBO J* **38**, (2019).
47. Fregno I, *et al.* ER-to-lysosome-associated degradation of proteasome-resistant ATZ polymers occurs via receptor-mediated vesicular transport. *EMBO J* **37**, (2018).

Figures

Figure 1

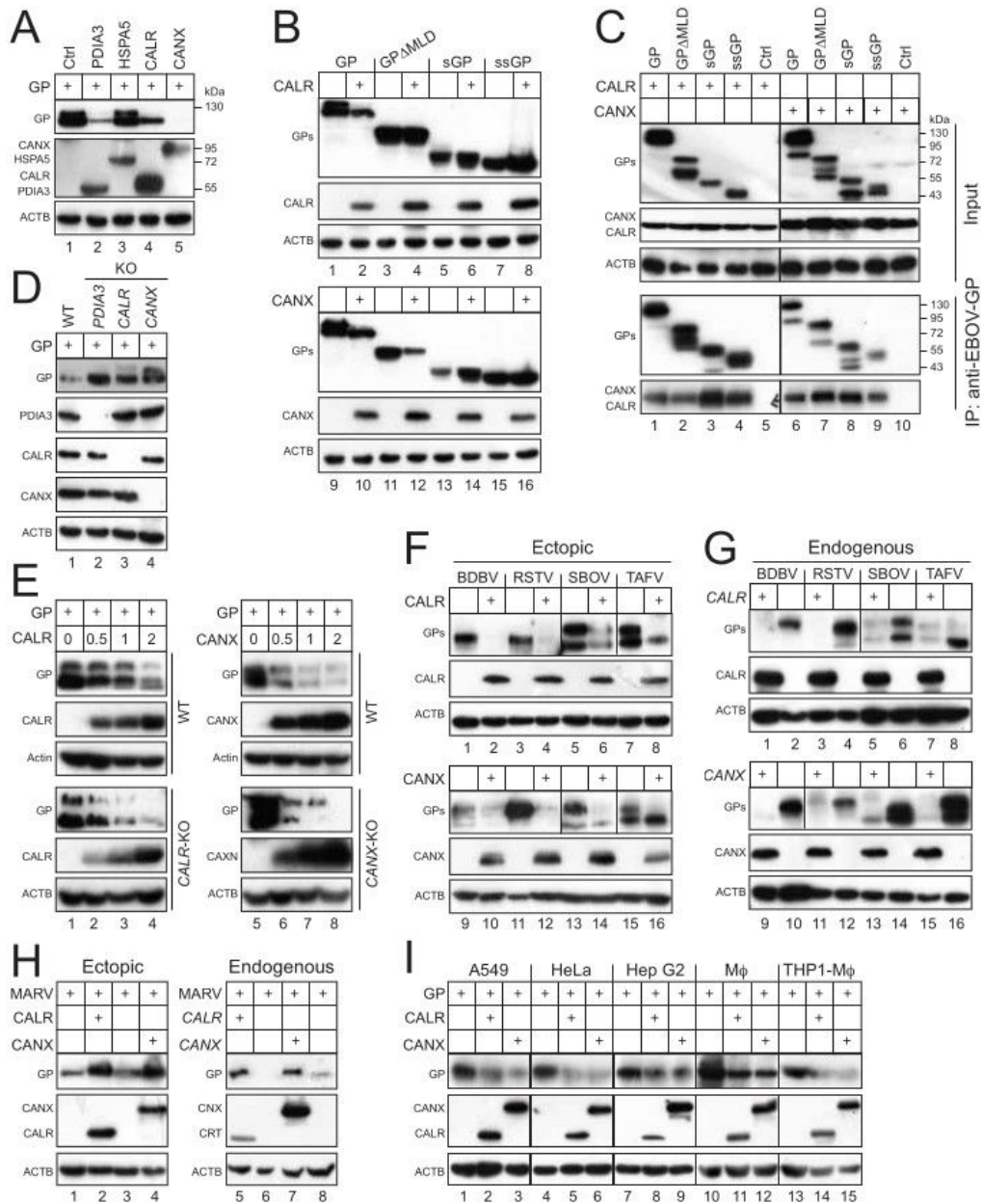


Figure 1

CANX and CALR decrease ebolavirus GP_{1,2} expression at steady state. **(A)** EBOV-GP_{1,2} (GP) was expressed with indicated ER proteins in HEK293T cells. Protein expression was detected by western blotting (WB). GP was detected by anti-EBOV-GP; PDIA3 and CALR were detected by anti-Myc; HSPA5 was detected by anti-FLAG; CANX was detected by anti-HA. Ctrl, control vector; ACTB, b-actin. **(B)** Indicated EBOV glycoproteins were expressed with CALR or CANX in HEK293T cells. Protein expression was

detected by WB. EBOV glycoproteins were detected by anti-HiBiT; CALR was detected by anti-Myc; CANX was detected by anti-HA. **(C)** Indicated EBOV glycoproteins were expressed with CANX or CALR in HEK293T cells, and co-immunoprecipitated (IP) with anti-EBOV-GP from cell lysate (Input). The GP interactions with CANX and CALR were determined by WB. GPs were detected by anti-EBOV-GP; CALR was detected by anti-Myc; CANX was detected by anti-HA. **(D)** EBOV-GP_{1,2} was expressed in HEK293T wild-type (WT) and *PDIA3*⁻, *CALR*⁻, or *CANX*-knockout (KO) cells. Protein expression was detected by WB. GP and endogenous PDIA3, CALR, and CANX were detected by their specific antibodies. **(E)** EBOV-GP_{1,2} was expressed with increased amounts of CALR or CANX in HEK293T WT and *CALR*⁻ or *CANX*-KO cells. Protein expression was detected by WB. GP was detected by anti-EBOV-GP; CALR and CANX were detected by anti-Myc or anti-HA. **(F)** GP_{1,2} proteins from indicated ebolaviruses were expressed with CALR or CANX in HEK293T cells. Protein expression was detected by WB. GPs were detected by anti-EBOV-GP; CALR and CANX were determined by anti-Myc or anti-HA. **(G)** GP_{1,2} proteins from indicated ebolaviruses were expressed in HEK293T WT and *CALR*⁻ or *CANX*-KO cells. Protein expression was detected by WB. GPs were detected by anti-EBOV-GP; CALR and CANX were detected by their specific antibodies. **(H)** MARV-GP_{1,2} was expressed with CANX or CALR in HEK293T cells. Alternatively, MARV-GP_{1,2} was expressed in HEK293T WT and *CALR*⁻ or *CANX*-KO cells. Protein expression was detected by WB. MARV-GP was detected by anti-HiBiT; ectopic CALR and CANX were detected by anti-Myc or anti-HA; endogenous CALR and CANX were detected by their specific antibodies. **(I)** EBOV-GP_{1,2} was expressed with CANX or CALR in A549 cells, HeLa cells, Hep G2 cells, primary mouse macrophages (Mf), and THP1-derived macrophages (THP1-Mf). Protein expression was detected by WB. GP was detected by anti-EBOV-GP; CALR and CANX were detected by anti-Myc or anti-HA.

Figure 2

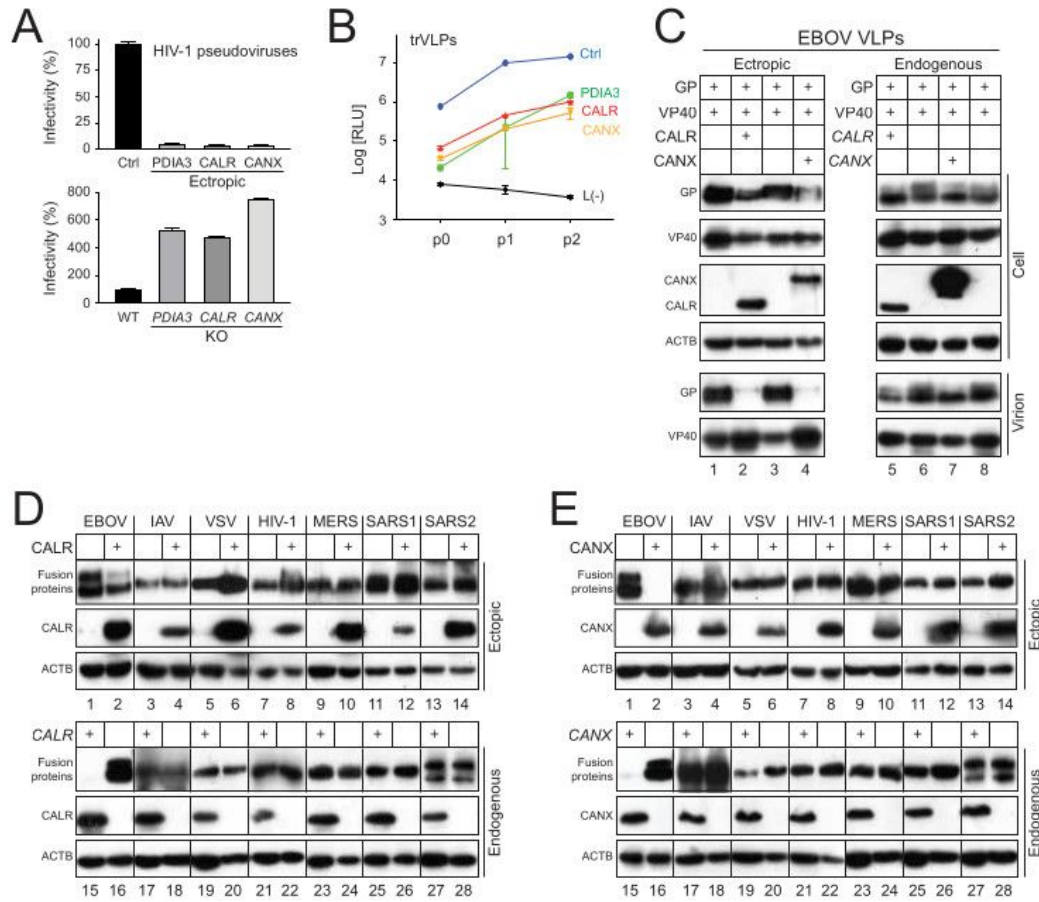


Figure 2

CANX and CALR reduce EBOV entry. (A) HIV-1 firefly luciferase reporter viruses pseudotyped with EBOV-GP_{1,2} were produced from HEK293T WT, PDIA3, CALR or CANX-overexpressing, and PDIA3-, CALR- or CANX-KO cells. After infecting HEK293T cells with an equal number of these different viruses, viral entry was determined by measuring intracellular luciferase activities. Viral entry is shown as relative values, with the entry of viruses produced from HEK293T WT cells in the presence of a control vector set to

100%. **(B)** EBOV replication and transcription-competent virus-like particles (trVLPs) were produced (p0) and passaged two times (p1, p2) in HEK293T cells in the presence or absence of PDIA3, CALR, or CANX. EBOV replication was determined by measuring intracellular *Renilla* luciferase activity. Viral replication was also measured in the absence of EBOV-L [L(-)], which served as a negative control. Results from three independent experiments are presented. **(C)** EBOV virus-like particles (VLPs) were produced from HEK293T WT, CALR or CANX-overexpressing, and *CALR*- or *CANX*-KO cells after expression of EBOV-GP_{1,2} with EBOV-VP40. VLPs were purified by ultra-centrifugation and protein expression in cell lysate and virions was analyzed by WB. GP, VP40, and endogenous CALR and CANX were detected by their specific antibodies; ectopic CALR and CANX were detected by anti-Myc or anti-HA. **(D)** Viral fusion proteins from indicated viruses were expressed with CALR in HEK293T cells (lanes 1-14). Alternatively, they were also expressed in HEK293T WT or *CALR*-KO cells (lanes 15-28). Protein expression was detected by WB. EBOV-GP_{1,2}, MERS-S, SRAS1-S, and SARS2-S were detected by anti-FLAG; IAV (H5N5) HA, VSV-G, HIV-1 Env, and CALR were detected by their specific antibodies. **(E)** Viral fusion proteins from indicated viruses were expressed with CANX in HEK293T cells (lanes 1-14). Alternatively, they were also expressed in HEK293T WT or *CANX*-KO cells (lanes 15-28). Protein expression was detected by WB as in **D**, except that CANX was detected by its specific antibody. Error bars in **A** and **B** represent the standard error of measurements (SEMs) calculated from three independent experiments. *p<0.05, **p<0.01, ***p<0.001, ****p<0.0001, ns (p>0.05).

Figure 3

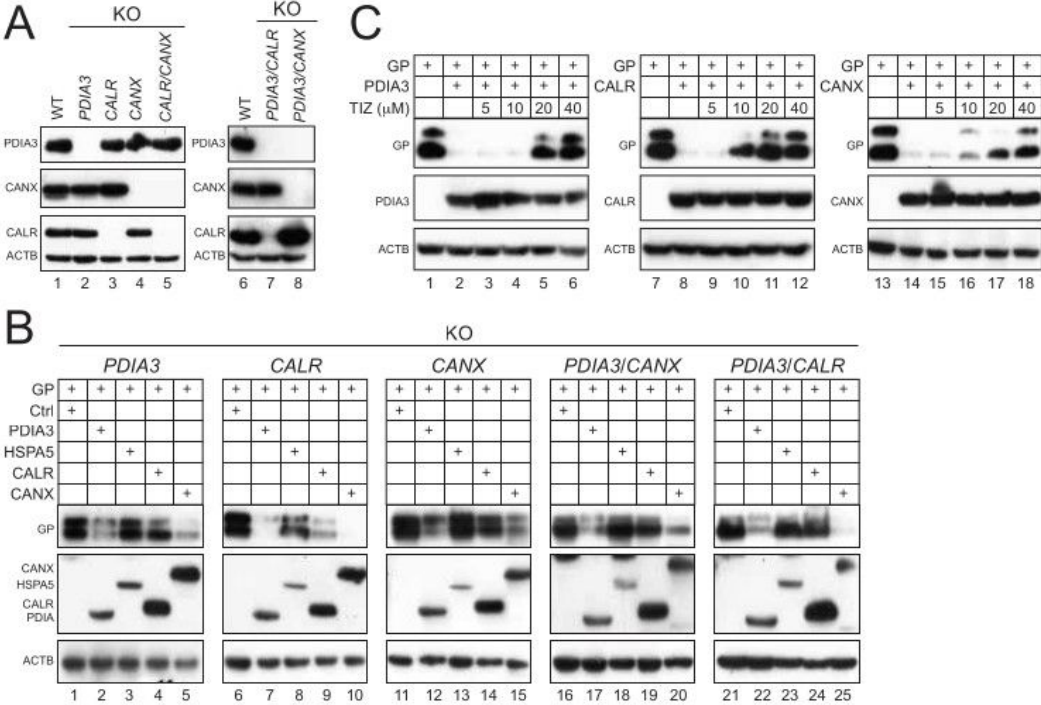


Figure 3

Interrelationship between CANX, CALR, and PDIA3 in EBOV-GP_{1,2} (GP) downregulation. **(A)** Expression of PDIA3, CALR, and CANX was determined in HEK293T WT, single *PDIA3*-, *CALR*-, or *CANX*-KO, and dual *PDIA3/CALR*- or *PDIA3/CANX*-KO cells. Protein expression was determined by WB. PDIA3, CALR, and CANX were detected by their specific antibodies. **(B)** GP was expressed with indicated ER proteins in HEK293T WT and indicated KO cells. Protein expression was detected by WB. GP was detected by anti-

EBOV-GP; PDIA3 and CALR were detected by anti-Myc; HSPA5 was detected by anti-FLAG; CANX was detected by anti-HA. (C) GP was expressed with PDIA3, CALR, or CANX in HEK293T cells. Cells were treated with indicated amounts of Tizoxanide (TIZ), and protein expression was determined by WB. GP was detected by anti-EBOV-GP; PDIA3 and CALR were detected by anti-Myc; CANX was detected by anti-HA.

Figure 4

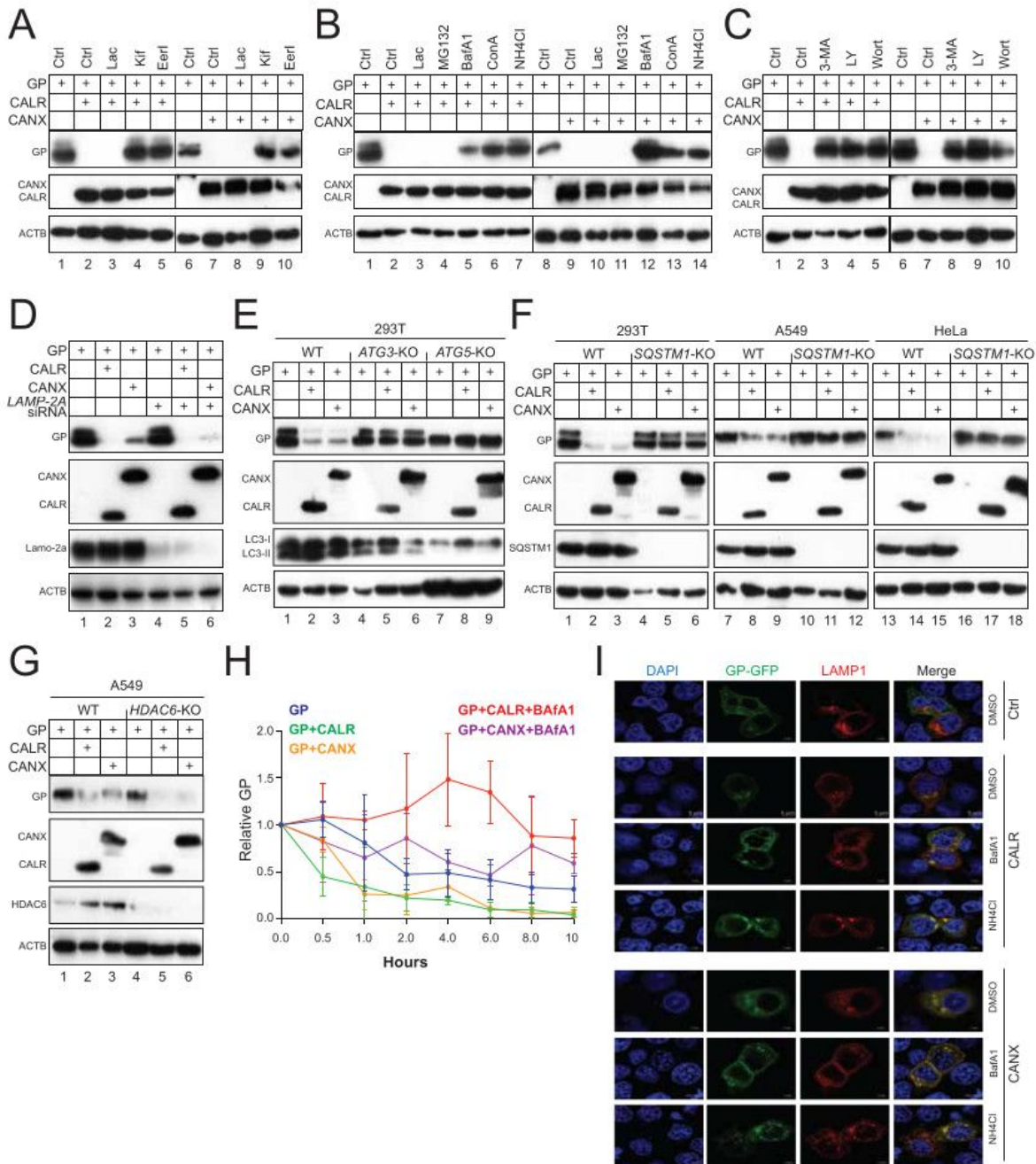


Figure 4

CALR and CANX target EBOV-GP_{1,2} (GP) to the lysosomes for degradation via ERAD machinery. **(A)** GP was expressed with CALR or CANX in HEK293T cells and treated with 20 mM lactacystin (Lac), 50 mM kifunensine (KIF), or 10 mM eeyarestatin I (EerI). DMSO was used as a vehicle control. Protein expression was detected by WB. GP was detected by anti-EBOV-GP; CALR and CANX were detected by anti-Myc or anti-HA. **(B)** GP was expressed with CALR or CANX in HEK293T cells and treated with 20 mM Lac, 20 mM MG132, 100 nM bafilomycin A1 (BafA1), 20 nM concanamycin A (ConA), or 20 mM NH₄Cl. DMSO was used as a vehicle control. Protein expression was detected by WB. GP was detected by anti-EBOV-GP; CALR and CANX were detected by anti-Myc or anti-HA. **(C)** GP was expressed with CALR or CANX in HEK293T cells and treated with 10 mM 3-methyladenine (3-MA), 20 mM LY294002 (LY), or 100 nM wortmannin (Wort). DMSO was used as a vehicle control (Ctrl). Protein expression was detected by WB. GP was detected by anti-EBOV-GP; CALR and CANX were detected by anti-Myc or anti-HA. **(D)** GP was expressed with CALR or CANX in HEK293T cells in the presence of *LAMP-2A*-siRNA. Protein expression was analyzed by WB. GP was detected by anti-EBOV-GP; CALR and CANX were detected by anti-Myc or anti-HA; LAMP-2A was detected by its specific antibody. **(E)** GP was expressed with CALR or CANX in HEK293T WT and *ATG3*- or *ATG5*-KO cells. Protein expression was analyzed by WB. GP was detected by anti-EBOV-GP; CALR and CANX were detected by anti-Myc or anti-HA; LC3 was detected by its specific antibody. **(F)** GP was expressed with CALR or CANX in indicated WT and *SQSTM1*-KO cells. Protein expression was analyzed by WB. GP was detected by anti-EBOV-GP; CALR and CANX were detected by anti-Myc or anti-HA; SQSTM1 was detected by its specific antibody. **(G)** GP was expressed with CALR or CANX in A549 WT and *HDAC6*-KO cells. Protein expression was analyzed by WB. GP was detected by anti-EBOV-GP; CALR and CANX were detected by anti-Myc or anti-HA; HDAC6 was detected by its specific antibody. **(H)** GP was expressed with CALR or CANX in HEK293T cells. Cells were treated with 50 μM cycloheximide (CHX) in the presence or absence of 100 nM BafA1. Cells were collected at indicated time points and protein expression was detected by WB. Levels of GP expression were quantified from the blots by ImageJ and are presented as relative values, with the values from time 0 set to 1. Error bars represent SEMs calculated from three independent experiments. **(I)** GP with a C-terminal GFP tag (GP-GFP) was expressed with LAMP1 that has a dsRed tag in the presence or absence of CALR or CANX in HeLa cells. Cells with ectopic CALR or CANX were treated with DMSO, 100 nM BafA1, or 20 mM NH₄Cl. The co-localization of EBOV-GP with LAMP1 was determined by confocal microscopy.

Figure 5

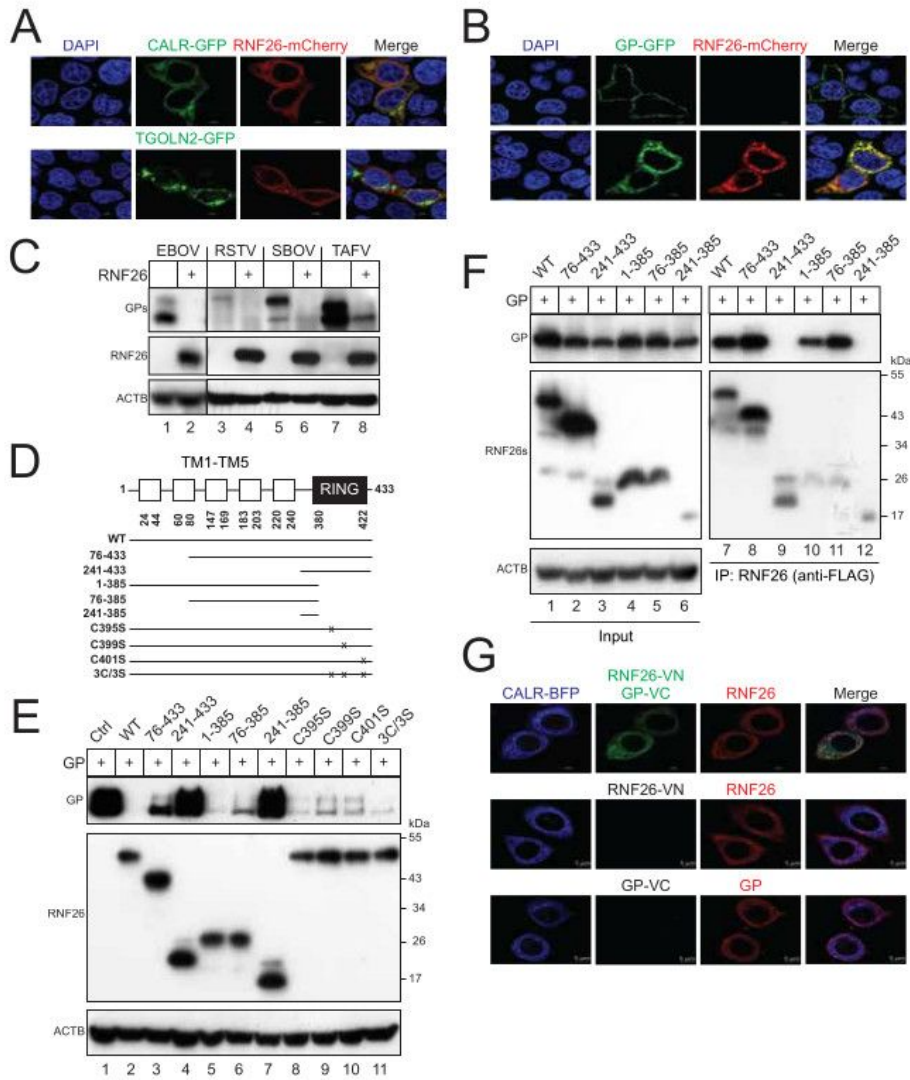


Figure 5

RNF26 decreases EBOV-GP_{1,2} expression in an E3 ubiquitin ligase activity-independent manner. (A) RNF26 with a C-terminal mCherry tag was expressed with CALR or TGOLN2 (Trans-Golgi network integral membrane protein 2) that has a GFP-tag in HeLa cells. The RNF26 subcellular localization was determined by confocal microscopy. (B) EBOV-GP_{1,2} (GP) with a C-terminal GFP tag was expressed with RNF26-mCherry in HeLa cells, and their co-localization was determined by confocal microscopy. (C) GP_{1,2}

proteins from indicated ebolaviruses were expressed with RNF26 in HEK293T cells. Protein expression was detected by WB. GPs were detected by anti-EBOV-GP; RNF26 was detected by anti-FLAG. **(D)** A schematic diagram of RNF26 is presented on the top. Five transmembrane (TM1-TM5) domains and a RING-finger are shown. Five RNF26 deletion mutants that target indicated regions and four point-mutation mutants that target each of C395, C399, or C401 are indicated. **(E)** EBOV-GP_{1,2} (GP) was expressed with RNF26 WT and its mutants in HEK293T cells. Protein expression was determined by WB. GP was detected by anti-EBOV-GP; RNF26 proteins were detected by anti-FLAG. **(F)** EBOV-GP_{1,2} (GP) with a HiBiT tag was expressed with RNF26 WT and its mutants in HEK293T cells. RNF26 proteins were immunoprecipitated and their interactions with GP was analyzed by WB. GP was detected by anti-EBOV-GP; RNF26 proteins were detected by anti-FLAG; GFP was detected by its specific antibody. **(G)** RNF26-VN and EBOV-GP_{1,2}-VC were expressed with CALR that has a C-terminal Blue Fluorescent Protein (BFP) tag in HeLa cells. RNF26 was stained with a red-fluorescent antibody. The subcellular localization of the RNF26-GP complex was determined by confocal microscopy.

Figure 6

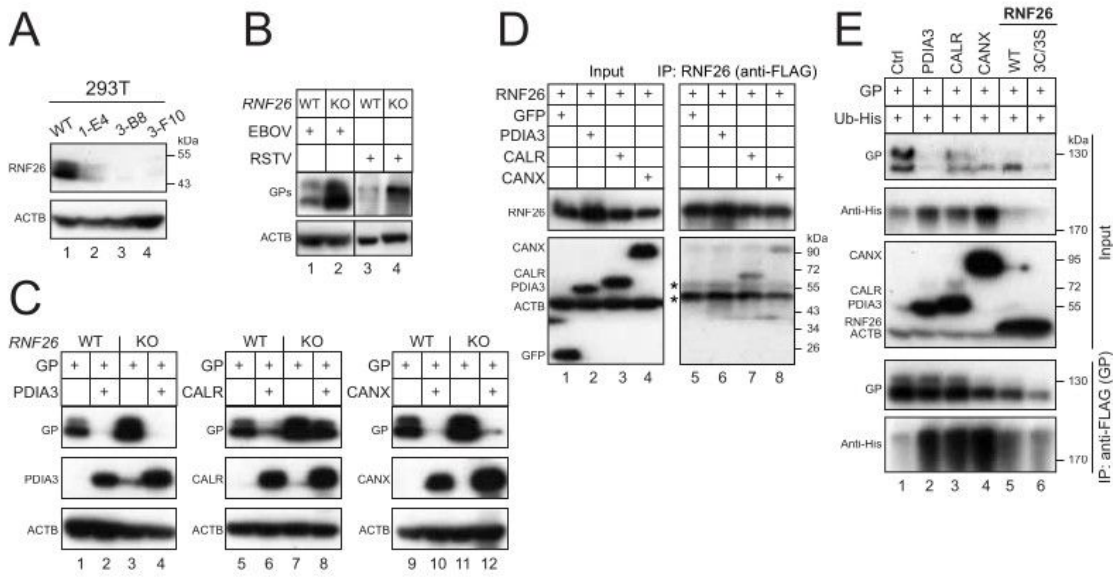


Figure 6

RNF26 selectively supports CALR, but not CANX or PDIA3. **(A)** Three *RNF26*-KO cell lines (1-E4, 3-B8, 3-F10) were generated from HEK293T cells using CRISPR/Cas9. RNF26 expression in these cells was determined by WB using its specific antibody. **(B)** EBOV and RSTV GP_{1,2} proteins were expressed in HEK293T WT and *RNF26*-KO (1-E4) cells. GP expression was detected by WB using anti-EBOV-GP. **(C)** EBOV-GP_{1,2} (GP) was expressed with PDIA3, CALR, or CANX in HEK293T WT and *RNF26*-KO (1-E4) cells.

Protein expression was detected by WB. GP was detected by anti-EBOV-GP; PDIA3 and CALR were detected by anti-Myc; CANX was detected by anti-HA. **(D)** RNF26 was expressed with GFP, PDIA3, CALR, or CANX in HEK293T cells. RNF26 was co-immunoprecipitated (IP) from cell lysate (Input) and its interactions with these proteins was determined by WB. GP was detected by anti-EBOV-GP; PDIA3 and CALR were detected by anti-Myc; CANX was detected by anti-HA; RNF26 was detected by anti-FLAG; GFP was detected by its specific antibody. **(E)** GP was expressed with His-tagged ubiquitin (Ub) and PDIA3, CALR, CANX, and RNF26 or its catalytically inactive mutant (3C/3S) in HEK293T cells. GP proteins were immunoprecipitated and GP polyubiquitination was determined by WB. GP was detected by anti-EBOV-GP; PDIA3 and CALR were detected by anti-Myc; CANX was detected by anti-HA; Ub was detected by anti-His.

Figure 7

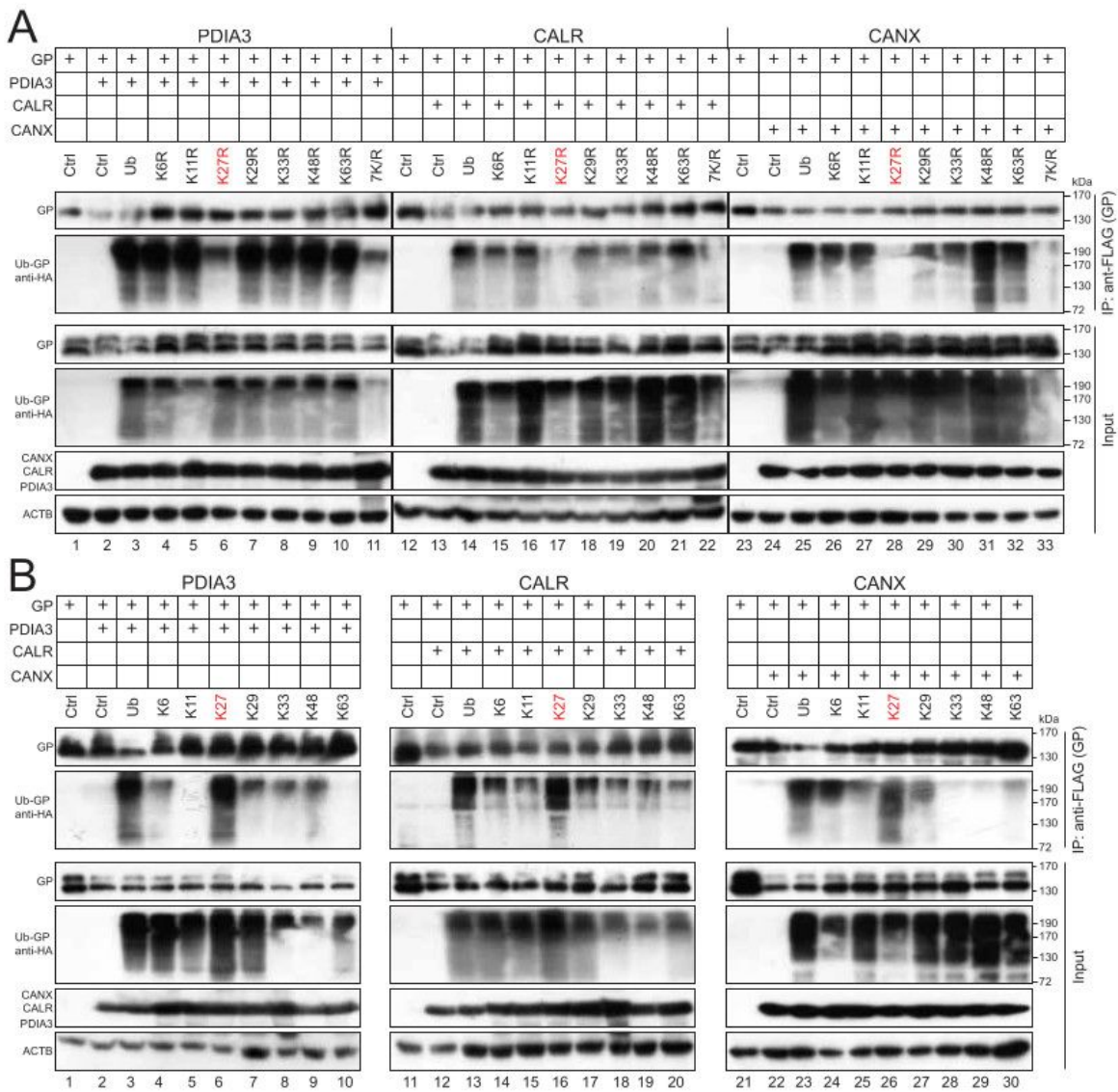


Figure 7

EBOV-GP_{1,2} (GP) is polyubiquitinated with K27-linked ubiquitin chains. **(A)** GP was expressed with Ub or its mutants bearing indicated single K-to-R mutation, and PDIA3, CALR, or CANX, in HEK293T cells. GP proteins were immunoprecipitated and GP polyubiquitination was analyzed by WB. **(B)** GP was expressed with Ub or its mutants expressing indicated single lysine residue, and PDIA3, CALR, or CANX, in HEK293T cells. GP proteins were immunoprecipitated and GP polyubiquitination was analyzed by WB. In **A** and **B**,

GP was detected by anti-EBOV-GP; PDIA3, CALR, and CANX were detected by anti-Myc; Ub was detected by anti-HA.

Figure 8

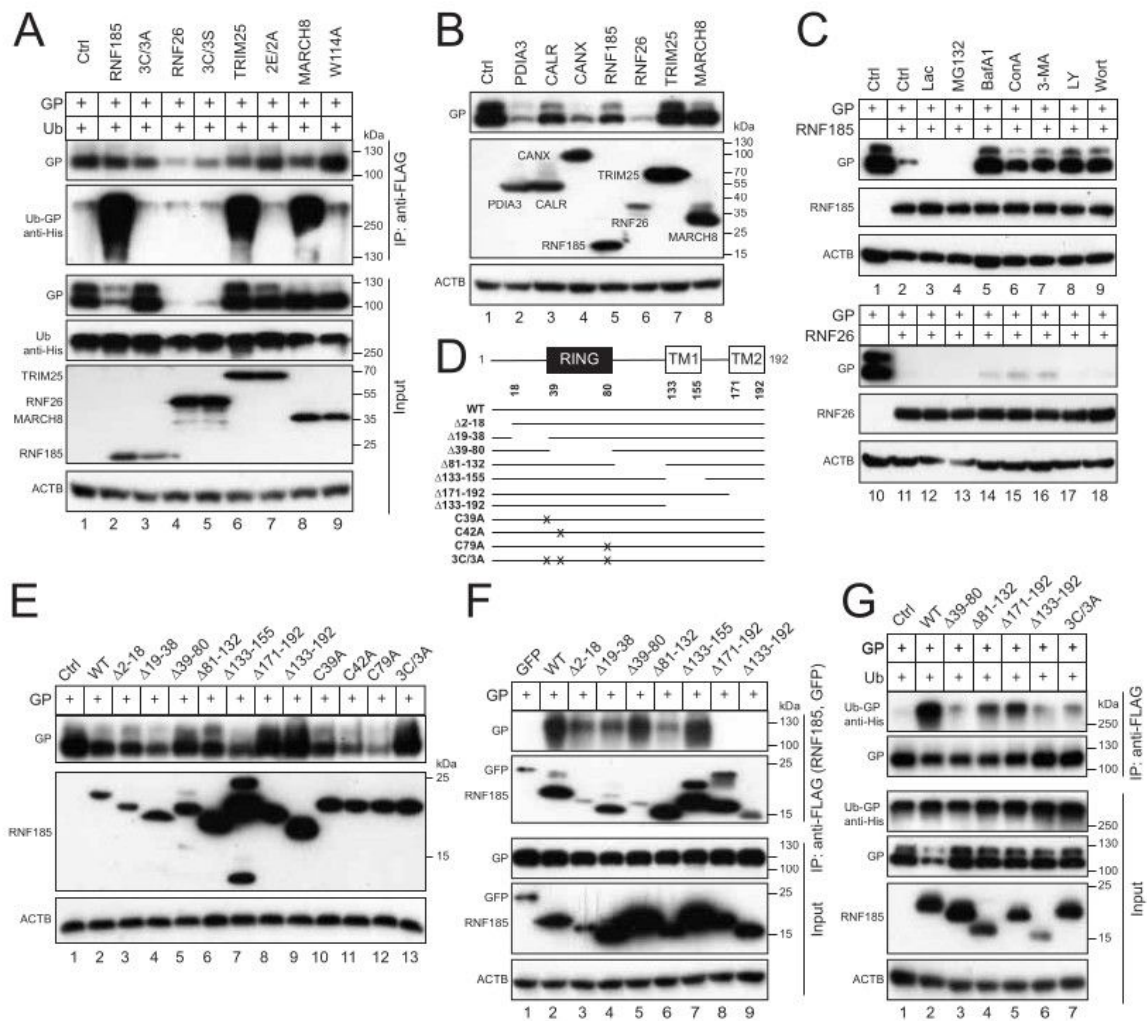


Figure 8

RNF185 polyubiquitinates and degrades EBOV-GP_{1,2} (GP). **(A)** GP was expressed with His-tagged Ub in the presence of indicated E3 Ub ligases or their catalytically inactive mutants in HEK293T cells. GP and E3 proteins were immunoprecipitated and GP polyubiquitination was analyzed by WB. GP was detected by anti-EBOV-GP; RNF26, RNF185, and TRIM25 were detected by anti-FLAG; MARCH8 was detected by anti-HA; Ub was detected by anti-His. **(B)** GP was expressed with indicated proteins in HEK293T cells. Protein expression was determined by WB. GP, RNF26, RNF185, TRIM25, and MARCH8 were detected as in **A**; PDIA3 and CALR were detected by anti-Myc; CANX was detected by anti-HA. **(C)** GP was expressed with RNF185 or RNF26 and treated with indicated inhibitors as we did previously. Protein expression was determined by WB. GP was detected by anti-EBOV-GP; RNF26 and RNF185 proteins were detected by anti-FLAG. **(D)** A schematic diagram of RNF185 is presented. Two transmembrane (TM1, TM2) domains and a RING-finger are shown. Indicated RNF26 mutants were constructed. **(E)** GP was expressed with RNF185 and its mutants in HEK293T cells. Protein expression was determined by WB. GP was detected by anti-EBOV-GP; RNF185 proteins were detected by anti-FLAG. **(F)** GP was expressed with GFP, RNF185, and indicated RNF185 mutants in HEK293T cells. GFP and RNF185 proteins were immunoprecipitated and their interaction with GP was analyzed by WB. GP was detected by anti-EBOV-GP; GFP and RNF185 proteins were detected by anti-FLAG. **(G)** GP was expressed with Ub with a His-tag and RNF185 or its indicated mutants in HEK293T cells. GP and RNF185 proteins were immunoprecipitated and GP polyubiquitination was determined by WB. GP was detected by anti-EBOV-GP; RNF185 proteins were detected by anti-FLAG; Ub was detected by anti-His.

Figure 9

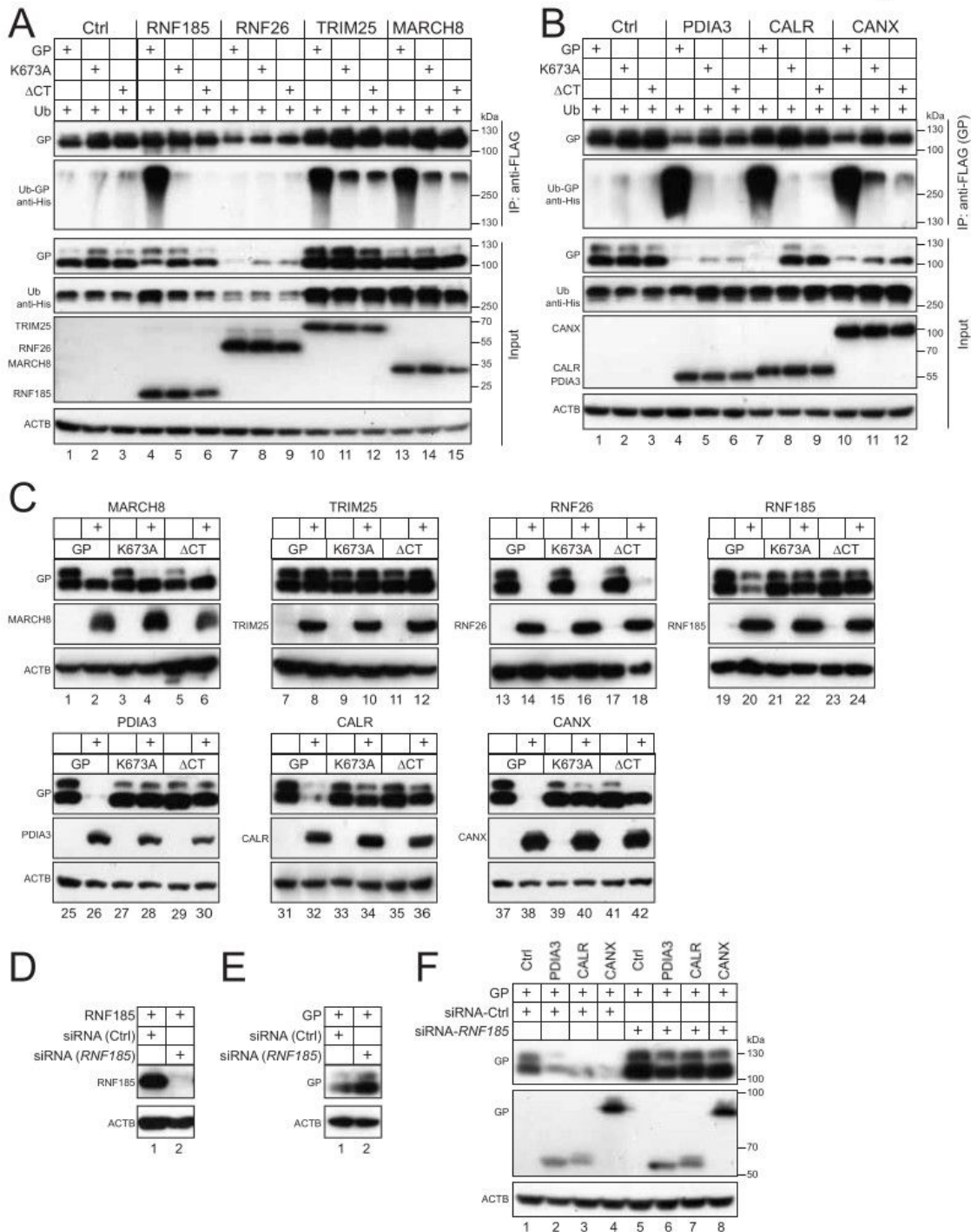


Figure 9

RNF185 polyubiquitinates EBOV-GP_{1,2} (GP) on K673 in the cytoplasmic tail. **(A)** GP and its mutants K673A or Δ CT were expressed with indicated E3 Ub ligases in HEK293T cells. GP and E3 proteins were immunoprecipitated and GP polyubiquitination was analyzed by WB. GP was detected by anti-EBOV-GP; RNF26, RNF185, and TRIM25 were detected by anti-FLAG; MARCH8 was detected by anti-HA; Ub was detected by anti-His. **(B)** GP and its two mutants were expressed with His-tagged Ub in the presence of

PDIA3, CALR, or CANX in HEK293T cells. GP proteins were immunoprecipitated and GP polyubiquitination was analyzed by WB. GP was detected by anti-EBOV-GP; PDIA3 and CALR were detected by anti-Myc; CANX was detected by anti-HA; Ub was detected by anti-His. **(C)** GP and its two mutants were expressed with indicated E3 ubiquitin ligases or ER proteins in HEK293T cells. Protein expression was determined by WB. GP was detected by anti-EBOV-GP; MARCH8 and CANX were detected by anti-HA; RNF26, RNF185, and TRIM25 were detected by anti-FLAG; PDIA3 and CALR were detected by anti-Myc. **(D)** RNF185 was expressed with a control (Ctrl) or *RNF185*-specific siRNAs in HEK293 cells. RNF185 expression was determined by WB using anti-FLAG. **(E)** GP was expressed with PDIA3, CALR, or CANX in the presence of Ctrl or *RNF185*-specific siRNAs in HEK293T cells. GP expression was determined by WB using anti-EBOV-GP. **(F)** GP was expressed with CALR, CANX, or PDIA3, and indicated siRNAs in HEK293T cells. GP expression was determined by WB using anti-EBOV-GP.

Figure 10

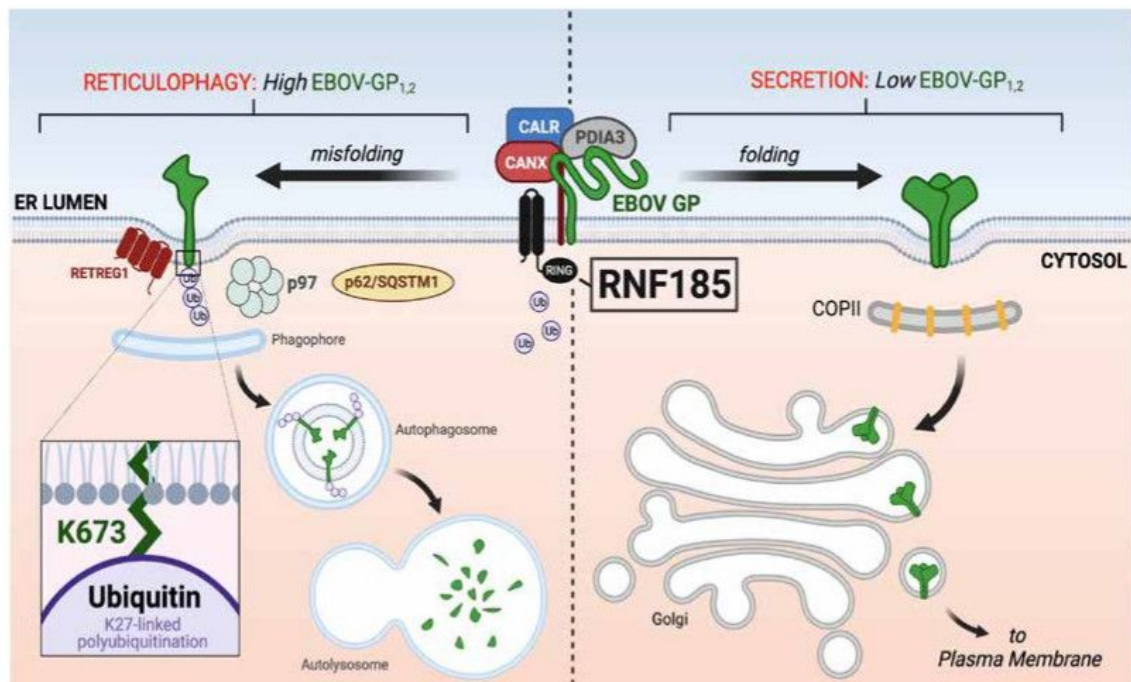


Figure 10

A model of how EBOV-GP_{1,2} expression is regulated in the ER via reticulophagy. When GP_{1,2} levels are low in the ER, CANX-CALR cycle promotes GP_{1,2} folding. Properly folded GP_{1,2} is released from the ER to the Golgi via COPII vesicles and secreted to the plasma membrane. However, when GP_{1,2} levels become high in the ER, the same CANX-CALR cycle starts to trigger GP_{1,2} misfolding. RNF185 polyubiquitinates

aberrant GP_{1,2} on K673 in the cytoplasmic tail via K27-linked ubiquitination. Polyubiquitinated GP_{1,2} is recruited to the phagophore assembly site by RETREG1 and packaged into autophagosomes via p97 ATPases and p62/SQSTM1, resulting in GP_{1,2} degradation in autolysosomes. Thus, CANX-CALR cycle promotes ebolavirus fitness in host cells by regulating GP_{1,2} expression levels during infection.